DISCLAIMER NOTICE

THIS DOCUMENT IS BEST QUALITY PRACTICABLE. THE COPY FURNISHED TO DTIC CONTAINED A SIGNIFICANT NUMBER OF PAGES WHICH DO NOT REPRODUCE LEGIBLY.

AEROELASTIC AND STRUCTURES RESEARCH LABORATORY
MASSACHUSETTS INSTITUTE OF TECHNOLOGY

TECHNICAL REPORT 72-1

RESPONSE AND LOADS ON AIRSHIPS DUE TO DISCRETE AND RANDOM GUSTS

BY
J. M. CALLIGEROS
P. W. McDAVITT

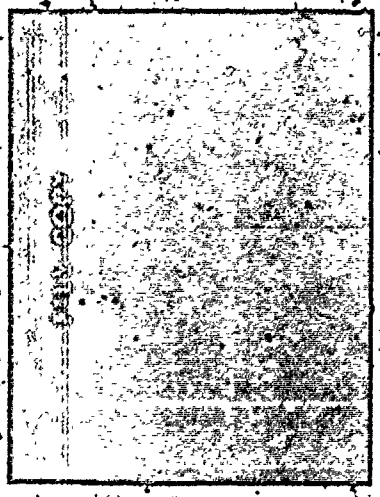

FOR THE
BUREAU OF AERONAUTICS
DEPARTMENT OF THE NAVY
CONTRACT NO. NOas 56-825-d

FEBRUARY 1958

AEROELASTIC AND STRUCTURES RESEARCH LABORATORY
MASSACHUSETTS INSTITUTE OF TECHNOLOGY

TECHNICAL REPORT 72-1

RESPONSE AND LOADS ON AIRSHIPS DUE TO DISCRETE AND RANDOM GUSTS

FOR THE
BUREAU OF AERONAUTICS
DEPARTMENT OF THE NAVY
CONTRACT NO. NOas 56-825-d

FEBRUARY 1958

REPORTED BY: J. M. Calligeros
J. M. Calligeros

P. W. McDavitt
P. W. McDavitt

APPROVED BY: T. H. H. Pian
T. H. H. Pian

ABSTRACT

The equations of motion of an airship encountering discrete and random gusts and expressions for the resulting structural loads are formulated. The aerodynamic forces and moments due to the gust and the resulting motion are derived from slender-body theory. Corrections are applied to account for viscous effects. A numerical example is presented to determine the response and loads of a typical airship penetrating a discrete one-minus-cosine gust and random turbulence. The discrete gust results indicate that critical loads on the envelope and tail are caused by a gust length equal to the length of the airship. The random gust results indicate that the critical scale of turbulence is also approximately one airship length. On the basis of these computations a rational procedure in airship gust load criteria is proposed.

ACKNOWLEDGEMENTS

The authors are indebted to the following people who have contributed to this report: Professor T. H. H. Pian, for his guidance and helpful suggestions as supervisor of the project; Mr. K. A. Fesz, for the many helpful discussions concerning various aspects of the project; Professor H. Ashley, for his advice on slender-body aerodynamics; Mr. Fred Wan, who prepared the figures and assisted with the mathematical analysis; Mrs. Ruth Lyon and the staff of the computational section of the Aeroelastic and Structures Research Laboratory who performed the computations; and Mrs. Iris G. Wheaton for typing the manuscript.

TABLE OF CONTENTS

LIST OF TABLES

LIST OF FIGURES

LIST OF SYMBOLS

$\mathfrak{M}$	Bending moment
C_L	Lift coefficient, based on $(\text{Volume})^{2/3}$
C_M	Pitching moment coefficient, based on $(\text{Volume})^{2/3}$
$\frac{D}{Dt}$	Substantial derivative, $\frac{\partial}{\partial t} + V_o \frac{\partial}{\partial x}$
$F_1(k)$	Steady-state lift function
$F_2(k)$	Steady-state Pitching moment function
$f_1(x)$	Apparent area of slender-body cross-section
$(f_2)_T$	$\int_0^{L_a} f_1(x)\,dx - (x_T - \bar{x}_{ca})(f_1)_T$
h	Vertical displacement of airship center of gravity
H	Transfer function or frequency response function
I_o	Airship pitching moment of inertia
$I_1, \ldots I_{11}$	Integrals dependent on the distributed apparent and physical mass of the airship
k	Reduced frequency of oscillation, $\frac{\omega L_a}{V_o}$
k_2	Coefficient of the additional apparent mass of the airship in the transverse direction
k_3	Coefficient of the additional pitching moment of inertia of the airship
L	Lift
L_a	Airship length
ℓ	Atmospheric scale of turbulence

M_o	Total mass of airship
M	Pitching moment
$m(x)$	Distributed mass of airship
m	Dimensionless parameter = $\frac{1}{\lambda}\left(\frac{k_2}{1+k_2}\right)$
n	Dimensionless parameter = $(Vol)^{1/3}/L_a$
P_T	Normal load at tail section
$p(x)$	Distributed loading due to aerodynamic and inertia forces
q	Dynamic pressure = $\frac{1}{2}\rho V_o^2$
r	L/l
r_1	$d(C_L)/d(\dot{\alpha}\ell/V_o) \Big/ dC_L/d\alpha$
r_2	$d(C_m)/d(\dot{\alpha}\ell/V_o) \Big/ dC_m/d\alpha$
R	Envelope radius
R_{Ai}	Maximum Envelope radius
S_f	Fin span
S	Shear
t	Distance travelled in airship lengths = $\frac{V_o t}{L_a}$
t_G	Gust gradient distance, distance to gust peak in airship lengths
t	Time from beginning of gust penetration
V_o	Airship forward velocity
Vol	Volume of airship
$w(x)$	Distributed weight of airship
W_G	Vertical velocity of gust
W_o	Peak value of vertical gust velocity
x	Longitudinal coordinate, measured from bow of airship
x_o	Shear and bending-moment station

α	Angle of attack
ζ	Nondimensional vertical displacement of the center of gravity $= \frac{h}{L_a}$
ζ_0	Amplitude of steady-state displacement
θ	Pitch angle of airship, positive nose up
θ_0	Amplitude of steady-state pitch angle
λ	Dimensionless mass parameter $= \frac{1}{2}\rho \frac{\partial C_L}{\partial \alpha} \frac{L_a (V_0 L)^{2/3}}{m_a (1+k_3)}$
μ	Dimensionless pitching inertia parameter $= \frac{1}{2}\rho \frac{\partial C_m}{\partial \alpha} \frac{L^2 (V_0 L)}{I_0 (1+k_3)}$
ξ	Nondimensional variable of integration $= \frac{x}{L_a}$
ξ_0	Nondimensional station for shear and bending moment, $\frac{x_0}{L_a}$
ρ	Mass density of air
τ	$\frac{(V_0 L)^{1/2}}{L_a}$
$\Phi(\omega)$	Power spectral density of disturbance
φ_{L_g}	Lift function due to gust
$\varphi_{L_{gs}}$	Growth of lift due to penetration of a sharp-edged gust
φ_{m_g}	Pitching moment function due to gust
$\varphi_{m_{gs}}$	Growth of pitching moment due to penetration of sharp-edged gust
$\varphi_{s_{gs}}$	Growth of shear due to penetration of a sharp-edged gust
$\varphi_{BM_{gs}}$	Growth of bending moment due to penetration of sharp-edged gust
ω	Circular frequency of oscillation

Subscripts

BM	Relating to bending moment
cg	Relating to airship center of gravity
CP	Relating to center of pressure of tail fin.

F	Relating to junction of fin leading edge and envelope
:M	Imaginary component of a complex quantity
L	Relating to lift
M	Relating to pitching moment
$\tilde{M}$	Relating to a point on the empennage
R	Real component of a complex quantity
S	Relating to shear
T	Relating to fin trailing edge

Notation

$\overline{(\ )}$	Root mean square value
$(\ )'$	Differentiation with respect to S
$\dot{(\ )}$	Differentiation with respect to t

CHAPTER 1

INTRODUCTION

1.1 Historical Background

Previous work on gust load analysis of airships is limited and scattered. The earliest significant investigation in this field was conducted by Munk (Refs. 1 and 2) who used potential theory to calculate the forces and moments on airship hulls in steady flow. Further theoretical treatments using non-viscous theories were pursued by Zahm (Ref. 3) and Upson and Klikoff (Ref. 4) who obtained essentially the same results as Munk. Some early applications of Munk's potential theory in determining the loads imposed by gusts on rigid airships are presented in Refs. 5 through 7.

An early attack on the origin of the forces acting on a body of revolution was made by Harrington in Ref. 8. Harrington determined experimentally the distribution of vorticity in the wake of the body from which he was able to calculate the lift by using Prandtl's lifting-line theory. His results compared favorably with measured values. In 1938 Kuethe (Ref. 9) used a water tank to determine the forces and moments on a model of the Akron-Macon class from the recorded lateral and pitching accelerations of the center of buoyancy. A gust with a velocity gradient was simulated by a flow in a channel normal to the path of the model.

Recent investigations into the nature of the forces acting on bodies of revolution were conducted by Allen and Perkins (Ref. 10) and refined by Kelly (Ref. 11) who determined the normal force and pitching moment for angles of attack beyond the range of potential theory. Their method considered the additional force generated by the viscosity of the cross-flow and their results agreed well with experiment. At about the same time Hill (Ref. 12)

developed a theory by which the loading was predicted by replacing the body surface with a vortex sheet.

Investigations of the lift and moment acting on a slender body performing unsteady motion were conducted both theoretically and experimentally by Ashley, Zartarian and Neilson (Ref. 13). Foss (Ref. 14) determined expressions for the growth of lift and moment acting on a slender body as it penetrates a discrete gust.

A theoretical investigation of airship gust loading was conducted by Flomenhoft (Ref. 15) who determined the transient motion of an airship in response to discrete gusts striking the fins.

1.2 Object of the Present Investigation

Current design methods for present day airships are based primarily on semi-empirical techniques. The envelope and fins are designed using the concept of a sharp-edged gust applied directly to the stern of the airship (Ref. 16). A more realistic analysis considering the transient effect resulting from the gradual penetration of the envelope into a gust front is not utilized.

It is the purpose of the present investigation to apply the new techniques which have been developed for airplanes to the response of airships to gusts. The gradual penetration of the airship into the gust front will be considered and the resulting responses and loads determined. Recently, the application of generalized harmonic analysis to the gust response of airplanes has enjoyed some measure of success. The determination of the response of airships to random gust disturbances appears to be more appropriate since, because of its large relative length, the airship may possibly encounter a succession of gusts rather than a single "critical gust".

The loads acting on a typical airship experiencing discrete and random gust disturbances will be determined and compared to the loads

obtained by the semi-empirical approach. On the basis of these calculations, critical design parameters for the envelope and empennage of non-rigid airships currently in operation will be derived.

CHAPTER II

EQUATIONS OF MOTION

The present problem is to determine the vertical and pitching motions and the structural loads of an airship resulting from a vertical gust disturbance W_G. This gust is considered uniform in the direction normal to the plane of motion of the airship. It is further assumed that during gust encounter the controls of the airship remain locked and its forward velocity V_o is constant.

The coordinate system of the airship in a disturbed condition is shown in Figure 1 where h is the vertical displacement of the center of gravity and θ the pitch angle, defined positive as shown. Let $p(x,t)$ be the distributed loading acting on the airship, then, for equilibrium in the vertical direction

$$\int_{body} p(x,t)\,dx = 0 \tag{2.1}$$

and for equilibrium of moments about the center of gravity

$$\int_{body} (x_{cg} - x)\,p(x,t)\,dx = 0 \tag{2.2}$$

The distributed loading is derived from a consideration of the disturbance, motion, and inertia forces acting on the airship and may be written as

$$p(x,t) = \frac{dL_M}{dx} + \frac{dL_G}{dx} - m(x)\left[\ddot{h} + (x_{cg} - x)\ddot{\theta}\right] \tag{2.3}$$

where dL_M/dx and dL_G/dx are the distributed aerodynamic forces due to motion and disturbance and $m(x)$ is the distributed mass of the airship. Substitution of Eq. (2.3) into Eqs. (2.1) and (2.2) results in the following statements of equilibrium:

$$M_a \ddot{h} = \int_{body} \left(\frac{dL_M}{dx} + \frac{dL_G}{dx}\right) dx = L_M + L_G \tag{2.4}$$

$$I_o \ddot{\theta} = \int_{body} (x_{cg} - x)\left(\frac{dL_M}{dx} + \frac{dL_G}{dx}\right) dx = M_M + M_G \tag{2.5}$$

where M_a is the mass of the airship and I_o the pitching moment of inertia about the center of gravity.

2.1 Aerodynamic Forces Due to Motion

2.1.1 Lift Due to Motion

The aerodynamic forces and moments acting on the airship performing unsteady motions will be derived by linearized slender-body theory. Slender-body theory was first applied by Munk (Ref. 1) to the calculation of the forces on airship hulls and later extended by R. T. Jones

to slender wings in steady flow, Ref. 18. An excellent review of its development and applications is given in Refs. 19 and 20. The major assumption made in slender-body theory is that the momentum of the flow in a plane normal to the free stream is the same as if this flow were two-dimensional. This assumption implies that the variations of the geometrical properties of the body in the stream direction are small and, also, that the angle of attack and resultant motions be restricted to small amplitudes. The force per unit axial distance acting on the body is equal to the substantial time rate of change of the momentum of the cross-flow. Referring to Figure 1 and assuming the angle of attack, $\alpha(x,t)$, to be small, the velocity of the cross-flow at section A-A is $V_o \alpha(x,t)$ and the momentum is $\rho f_1(x) V_o \alpha(x,t)$, where ρ is the mass density of the fluid, $f_1(x)$ the apparent area of the cross-section, and V_o the free stream velocity. Therefore, the force per unit distance acting on the airship because of its motion, positive upward, is

$$\frac{dL_m}{dx} = \frac{D}{Dt}\left[\rho f_1(x) V_o \alpha(x,t)\right] \tag{2.6}$$

Within the limitations of slender-body theory, the substantial derivative has the form $\left(\frac{\partial}{\partial t} + V_o \frac{\partial}{\partial x}\right)$ and Eq. (2.6) becomes

$$\frac{dL_m}{dx} = \left(\frac{\partial}{\partial t} + V_o \frac{\partial}{\partial x}\right)\left[\rho f_1(x) V_o \alpha(x,t)\right] \tag{2.7}$$

where the angle of attack at each cross-section is

$$\alpha(x,t) = \theta - \frac{\dot{h}}{V_o} + (x - x_{cg})\frac{\dot{\theta}}{V_o} \tag{2.8}$$

Substituting Eq. (2.8) into Eq. (2.7) and differentiating, the lift due to motion per unit length is

$$\frac{dL_M}{dx} = 2q\left\{\left(\theta - \frac{\dot{h}}{V_0}\right)\frac{df_1(x)}{dx} + \frac{\dot{\theta}}{V_0}\left[2f_1(x) + (x - x_{CG})\frac{df_1(x)}{dx}\right]\right.$$

$$\left. - \frac{\ddot{h}}{V_0^2} f_1(x) - \frac{\ddot{\theta}}{V_0^2}(x_{CG} - x) f_1(x)\right\} \tag{2.9}$$

where $q = \frac{1}{2}\rho V_0^2$. Integrating Eq. (2.9) along the length of the airship, the total lift due to motion is

$$L_M = 2q\left\{\left(\theta - \frac{\dot{h}}{V_0}\right)(f_1)_T + \frac{\dot{\theta}}{V_0}\left[(f_1)_T (x_T - x_{CG})\right]\right.$$

$$\left. + \frac{\dot{\theta}}{V_0}\int_0^{L_a} f_1(x)dx - \frac{\dot{h}}{V_0^2}\int_0^{L_a} f_1(x)dx - \frac{\ddot{\theta}}{V_0^2}\int_0^{L_a}(x_{CG} - x) f_1(x)dx\right\} \tag{2.10}$$

In applying the limits of integration to the first and second terms of Eq. (2.9) the upper limit is taken as the location of the section of maximum span of the tail fin, $x = x_T$, because the turbulent nature of the flow aft of this section disrupts the two-dimensional idealization of the cross-flow (Ref. 18). The quantity $\rho\int_0^{L_a} f_1(x)\,dx$ is recognized as the apparent mass of the airship and may be written as a multiple of the physical mass, $k_2 M_a$, where k_2 is the coefficient of additional apparent mass in the transverse direction. The quantity $-\int_0^{L_a}(x_{CG} - x) f_1(x)\,dx$ is approximately zero

because $f_1(x)$ is symmetrically distributed about the center of gravity; hence the final term in Eq. (2.10) will be omitted. With these modifications Eq. (2.10) may be rewritten as

$$L_M = 2q\left[\left(\theta - \frac{\dot{h}}{V_0}\right)(f_1)_T + \frac{\dot{\theta}}{V_0}(f_1)_T (x_T - x_{CG})\right] + k_2 M_a V_0 \dot{\theta} - k_2 M_a \ddot{h} \tag{2.11}$$

where $(f_1)_T$ is the value of the apparent area of the cross-section at $x = x_T$.

2.1.2 Pitching Moment Due to Motion

The pitching moment due to motion about the center of gravity is

$$M_M = \int_{body} (x_{CG} - x)\frac{dL_M}{dx}\,dx \tag{2.12}$$

Substituting Eq. (2.9) in Eq. (2.12) and integrating up to $x = x_T$ as in Eq. (2.10)

$$M_M = 2\rho\left\{\left(\theta - \frac{\dot{h}}{V_0}\right)\left[\int_0^{L_a} f_1(x)\,dx - (x_T - x_{CG})(f_1)_T\right]\right.$$

$$- \frac{\dot{\theta}}{V_0}(x_T - x_{CG})^2 (f_1)_T - \frac{\dot{\theta}}{V_0^2}\int_0^{L_a} (x_{CG} - x)^2 f_1(x)\,dx$$

$$\left. - \frac{\ddot{h}}{V_0^2}\int_0^{L_a} (x_{CG} - x) f_1(x)\,dx\right\} \qquad (2.13)$$

The quantity $\rho\int_0^{L_a}(x_{CG} - x)^2 f_1(x)\,dx$ is the apparent pitching moment of inertia of the airship and may be rewritten as $k_3 I_0$, where k_3 is the coefficient of additional pitching moment of inertia. Neglecting the last term of Eq. (2.13) as in the case for lift, the pitching moment due to motion becomes

$$M_M = 2\rho\left\{\left(\theta - \frac{\dot{h}}{V_0}\right)\left[\int_0^{L_a} f_1(x)\,dx - (x_T - x_{CG})(f_1)_T\right]\right.$$

$$\left. - \frac{\dot{\theta}}{V_0}(x_T - x_{CG})^2 (f_1)_T\right\} - k_3 I_0 \ddot{\theta} \qquad (2.14)$$

2.2 Stability Derivatives from Slender Body Theory

By defining coefficients of lift and moment as

$$C_L = \frac{LIFT}{\frac{1}{2}\rho (V_{OL})^{2/3}} \tag{2.15}$$

$$C_M = \frac{MOMENT}{\frac{1}{2}\rho (V_{OL})^{2/3} L_a} \tag{2.16}$$

the following aerodynamic stability derivatives are obtained from Eqs. (2.11) and (2.14):

$$\frac{\partial C_L}{\partial \alpha} = \frac{2 (f_1)_T}{(V_{OL})^{2/3}}$$

$$\frac{\partial C_L}{\partial (\tau \dot{\theta})} = 2 (x_T - x_{CG}) \frac{\overline{(f_1)}_T}{V_{OL}}$$

$$\frac{\partial C_M}{\partial \alpha} = 2 \frac{(f_2)_T}{V_{OL}}$$

$$\frac{\partial C_M}{\partial (\tau \dot{\theta})} = -2 (x_T - x_{CG})^2 \frac{(f_1)_T}{(V_{OL})^{4/3}}$$

(2.17)

where

$$\tau = \frac{(V_{OL})^{1/3}}{V_o}$$

$$(f_2)_T = \int_0^{L_a} f_1(x)\, dx - (x_T - x_{CG})(f_1)_T \qquad (2.18)$$

Instead of using stability derivatives as expressed by Eqs. (2.17) above, values based on current design practice which include viscosity effects may be used. Therefore, a more rational approach in expressing the lift and moment due to motion at small angles of attack, is to write Eqs. (2.11) and (2.14) as

$$L_M = \rho (V_{OL})^{2/3} \frac{dC_L}{d\alpha}\left(\theta - \frac{\dot{h}}{V_o}\right) + q (V_{OL}) \frac{dC_L}{d(\tau\dot{\theta})} \frac{\dot{\theta}}{V_o} + k_2 M_a V_o \dot{\theta} - k_2 M_a \ddot{h}$$

$$M_M = q (V_{OL}) \frac{dC_M}{d\alpha}\left(\theta - \frac{\dot{h}}{V_o}\right) + q (V_{OL})^{4/3} \frac{dC_M}{d(\tau\dot{\theta})} \frac{\dot{\theta}}{V_o} - k_3 I_o \ddot{\theta} \qquad (2.19)$$

A comparison is given in Table I of the stability derivatives obtained from Eqs. (2.17) and by semi-empirical means for the example airship of Chapter IV. The theoretical values exceed the empirical values by

approximately five to fifteen percent, which may be attributed to the neglect of viscosity in slender body theory. The values given in column 8 will be used in this report.

2.3 Aerodynamic Forces Due to The Gust Disturbance

The lift due to a vertical gust disturbance may be found by considering $W_G(x,t)$ as the cross-flow velocity. Replacing $V_o a(x,t)$ by $W_G(x,t)$ in Eq. (2.6), the lift per unit distance due to the gust disturbance, positive upward, is

$$\frac{dL_G}{dx} = \frac{D}{Dt}\left[\rho f_i(x) W_G(x,t)\right]$$

$$=$$

$$\frac{dL_G}{dx} = \rho\left[f_i(x)\frac{D}{Dt} W_G(x,t) + W_G(x,t)\frac{Df_i(x)}{Dt}\right] \tag{2.20}$$

It is assumed that the gust profile does not change with time but travels along the x-direction with a uniform velocity V_o and is defined by the relationship

$$W_G(x,t) = W_G(V_o t - x) \tag{2.21}$$

This relationship is a solution of the general wave equation and has the property

$$\frac{D}{Dt} W_G(V_o t - x) = \left(\frac{\partial}{\partial t} + V_o \frac{\partial}{\partial x}\right) W_G(V_o t - x) = 0 \tag{2.22}$$

which simplifies Eq. (2.20) to

$$\frac{dL_G}{dx} = \rho W_G V_o \frac{df_i(x)}{dx} = 2q \frac{W_o}{V_o} \frac{W_G}{W_o} \frac{df_i(x)}{dx} \tag{2.23}$$

where W_o is the amplitude of the gust profile. Integrating Eq. (2.23), the total lift due to the gust disturbance is

$$L_G = 2q \frac{W_o}{V_o} \int_{body} \frac{W_G(V_o t - x)}{W_o} \frac{df_i(x)}{dx} dx \tag{2.24}$$

and the pitching moment about the center of gravity, positive nose up, is

$$M_G = 2q \frac{W_o}{V_o} \int_{body} (x_{cg} - x) \frac{W_G(V_o t - x)}{W_o} \frac{df_i(x)}{dx} dx \tag{2.25}$$

In terms of the expressions for $dC_L/d\alpha$ and $dC_M/d\alpha$ given by Eq. (2.17), Eqs. (2.24) and (2.25) may be rewritten as

$$L_G = q(V_{OL})^{2/3} \frac{dC_L}{d\alpha} \frac{W_o}{V_o} \varphi_{L_G}$$

$$M_G = q(V_{OL}) \frac{dC_M}{d\alpha} \frac{W_o}{V_o} \varphi_{M_G} \tag{2.26}$$

where

$$\varphi_{L_{\dot{\alpha}}} = \frac{1}{(f_1)_T} \int_{body} \frac{W_G(V_0 t - x)}{W_0} \frac{df_1(x)}{dx} dx$$

$$\varphi_{M_{\dot{\alpha}}} = \frac{1}{(f_2)_T} \int_{body} (x_{CG} - x) \frac{W_G(V_0 t - x)}{W_0} \frac{df_1(x)}{dx} dx \tag{2.27}$$

As before, more realistic values for $dC_L/d\alpha$ and $dC_m/d\alpha$ may be used in Eqs. (2.26) in place of the values obtained by slender-body theory, Eqs. (2.17).

2.4 The General Equations of Motion

The equations of motion of the airship in disturbed flight, Eqs. (2.4) and (2.5), become

$$M_a(1+k_3)\ddot{h} - \rho(V_{0L})^{2/3}\left[\frac{dC_L}{d\alpha}\left(\theta - \frac{\dot{h}}{V_0}\right) + (V_{0L})^{1/3}\frac{dC_L}{d(z\dot{\theta})}\frac{\dot{\theta}}{V_0}\right]$$

$$-k_2 M_a V_0 \dot{\theta} = \rho(V_{0L})^{2/3}\frac{dC_L}{d\alpha}\frac{W_0}{V_0}\varphi_{L_G}$$

$$I_c(1+k_3)\ddot{\theta} - \rho(V_{0L})\left[\frac{dC_m}{d\alpha}\left(\theta - \frac{\dot{h}}{V_0}\right) + (V_{0L})^{1/3}\frac{dC_m}{d(z\dot{\theta})}\right] =$$

$$\rho(V_{0L})\frac{dC_m}{d\alpha}\frac{W_0}{V_0}\varphi_{M_G} \tag{2.28}$$

These equations may be simplified by introducing the nondimensional time variable $s = V_0 t / L_a$, which is the airship length travelled, and the nondimensional vertical displacement $\zeta = -h / L_a$. In transforming to the new time variable s, the following relationships also hold

$$\dot{h} = \frac{dh}{ds}\frac{ds}{dt} = \frac{V_0}{L_a} h' = V_0 \zeta'$$

$$\ddot{h} = \frac{V_0^2}{L_a} \zeta''$$

$$\dot{\theta} = \frac{V_0}{L_a} \theta'$$

$$\ddot{\theta} = \left(\frac{V_0}{L_a}\right)^2 \theta''$$

(2.29)

where $(\,)'$ denotes differentiation with respect to s. Furthermore, the physical and aerodynamic characteristics of the airship may be represented by the following dimensionless parameters

$$\lambda = \frac{1}{2}\rho \frac{dC_L}{d\alpha} \frac{L_a (Vol)^{2/3}}{M_a (1+k_2)} \qquad \mu = \frac{1}{2}\rho \frac{dC_m}{d\alpha} \frac{L_a^2 (Vol)}{I_a (1+k_3)}$$

$$\tau_1 = \frac{dC_L/d(\tau\dot{\theta})}{dC_L/d\alpha} \qquad \tau_2 = \frac{dC_m/d(\tau\dot{\theta})}{dC_m/d\alpha}$$

$$m = \frac{1}{\lambda}\left(\frac{k_a}{1+k_2}\right) \qquad m = \frac{(Vol)^{1/3}}{L_a}$$

(2.30)

In terms of the new time variable s and the parameters given in Eq. (2.30) above, the equations of motion of the airship in nondimensional form become

$$\frac{1}{\lambda}\zeta'' + \zeta' - (m + m\lambda_1)\theta' - \theta = \frac{w_0}{V_0}\varphi_{L_G}$$

$$\frac{1}{\mu}\theta'' - m\lambda_2\theta' - \theta + \zeta' = \frac{w_0}{V_0}\varphi_{M_G} \tag{2.31}$$

where

$$\varphi_{L_G} = \frac{1}{(f_1)_T}\int_{body} \frac{w_G(s-\xi)}{w_0}\,\frac{df_1(\xi)}{d\xi}\,d\xi \tag{2.32}$$

$$\varphi_{M_G} = \frac{1}{(f_2)_T}\int_{body} (\xi_{cg} - \xi)\,\frac{w_G(s-\xi)}{w_0}\,\frac{df_1(\xi)}{d\xi}\,d\xi \tag{2.33}$$

and $\xi = \dfrac{x}{L_a}$.

2.5 Discrete Gust Excitation

In the discrete gust analysis, it is convenient to determine first the growths of lift and moment acting on the airship as it penetrates a sharp-edged gust. The growths of lift and moment due to any desired gust profile may then be obtained by applying Duhamel's integral to the sharp-edged gust functions.

The growth of lift due to a sharp-edged gust, $\varphi_{L_{GO}}$, is obtained from Eq. (2.3) by putting $\frac{W_0(1-\bar{\xi})}{W_0} = 1.0$ and integrating up to the gust front $\bar{s}$:

$$\varphi_{L_{GO}}(\bar{s}) = \frac{1}{(f_1)_T}\int_0^{\bar{s}} \frac{df_1(\bar{\xi})}{d\bar{\xi}}\, d\bar{\xi} = \frac{f_1(\bar{s})}{(f_1)_T} \qquad 0 \le \bar{s} \le \bar{\xi}_T$$

$$\varphi_{L_{GO}}(\bar{s}) = 1.0 \qquad \bar{s} \ge \bar{\xi}_T \tag{2.34}$$

Thus the lift acting on an airship as it penetrates a sharp-edged gust varies with the apparent area of the cross-section at the gust front. Similarly, the growth of moment due to a sharp-edged gust, $\varphi_{M_{GO}}$, is obtained from Eq. (2.33)

$$\varphi_{M_{GO}} = \frac{L_a}{(f_2)_T}\int (\bar{\xi}_{CG} - \bar{\xi}) \frac{df_1(\bar{\xi})}{d\bar{\xi}}\, d\bar{\xi}$$

(2.35)

which, after integrating by parts, yields

$$\varphi_{M_{GO}}(\bar{s}) = \frac{L_a}{(f_2)_T}\left[(\bar{\xi}_{CG} - \bar{s}) f_1(\bar{s}) + \int_0^{\bar{s}} f_1(\bar{\xi})\, d\bar{\xi}\right] \qquad 0 \le \bar{s} \le \bar{\xi}_T$$

$$\varphi_{M_{GO}}(\bar{s}) = 1.0 \qquad \bar{s} \ge \bar{\xi}_T \tag{2.36}$$

The growths of lift and moment due to an arbitrary discrete gust profile, $W_e(\bar{s})/W_0$ are obtained by applying Duhamel's integral to the indicial functions of Eqs. (2.34) and (2.36):

$$\varphi_{L_G}(s) = \frac{W_G(0)}{W_0}\,\varphi_{L_{G0}}(s) + \int_0^s \frac{d}{d\sigma}\left[\frac{W_G(\sigma)}{W_0}\right]\varphi_{L_{G0}}(s-\sigma)\,d\sigma \tag{2.37}$$

$$\varphi_{M_G}(s) = \frac{W_G(0)}{W_0}\,\varphi_{M_{G0}}(s) + \int_0^s \frac{d}{d\sigma}\left[\frac{W_G(\sigma)}{W_0}\right]\varphi_{M_{G0}}(s-\sigma)\,d\sigma \tag{2.38}$$

where σ is a dummy variable of integration. Knowing the forcing functions $\varphi_{L_G}(s)$ and $\varphi_{M_G}(s)$ it is then possible to solve the coupled equations of motion, Eqs. (2.31), for the responses $\zeta(s)$ and $\theta(s)$. Since the airship is at rest prior to disturbance, the accompanying initial conditions at $s = 0$ are

$$\zeta(0) = \zeta'(0) = \theta(0) = \theta'(0) = 0 \tag{2.39}$$

2.6 Random Gust Excitation

The response of the airship to random gust excitations may be determined by applying the concepts of generalized harmonic analysis which are discussed in Refs. 21 through 23. With the application of these concepts the response of the airship can be described in terms of statistical or average quantities, the most important of which is the mean square value. It is assumed that the gust turbulence is a stationary random process possessing the properties of homogeneity and isotropy. Stationarity and homogeneity imply that the statistical characteristics of the turbulence are invariant with

time and space, respectively. Isotropy implies that the statistical properties of the turbulence are independent of the airship flight path.

It has been shown (Ref. 21) that the mean square value of a response of a linear system, $\overline{\sigma_R^2}$, may be found from the following relationship:

$$\overline{\sigma_R^2} = \int_0^\infty |H_R(i\omega)|^2 \Phi(\omega)\, d\omega \tag{2.40}$$

where $H_R(i\omega)$ is the transfer function or frequency response function of the system, and $\Phi(\omega)$ is the power spectral density of the disturbance, both functions of the harmonic frequency ω. The output σ_R may be any response of the system such as velocity, acceleration or stress. The transfer function is the ratio of the amplitude of the system response to the amplitude of a sinusoidal forcing function.

As in previous theoretical studies of air turbulence (Refs. 22 and 23) the power spectral density of the vertical gust velocity will be approximated by

$$\Phi(\omega) = \overline{W_G^2}\,\frac{\ell}{\pi V_0}\,\frac{1+3\left(\frac{\omega\ell}{V_0}\right)^2}{\left[1+\left(\frac{\omega\ell}{V_0}\right)^2\right]^2} \tag{2.41}$$

where $\overline{W_G^2}$ is the mean square value of the vertical gust velocity and ℓ is the scale of turbulence, which can be considered as an approximate measure of the average eddy size in the turbulence. The transfer function of the airship is found by subjecting it to a continuous sinusoidal gust pattern of the form

$$\frac{w_G}{w_0}(x,t) = e^{i\frac{\omega}{V_0}(V_0 t - x)}$$

(2.42)

Equations (2.41) and (2.42) may be rewritten in terms of the reduced frequency parameter $k = \frac{\omega L_a}{V_0}$ as

$$\Phi(k,\lambda) = \overline{w_G^2}\frac{L_a}{\pi V_0}\frac{(\lambda^2+3k^2)\lambda}{(\lambda^2+k^2)^2}$$

(2.43)

$$\frac{w_G}{w_0} = e^{ik(\lambda-\xi)}$$

(2.44)

where $\lambda = 4/\ell$. The steady state lift and moment functions are obtained by substituting Eq. (2.44) into Eqs. (2.32) and (2.33),

$$\mathcal{L}_G(k,\lambda) = F_1(k)\,e^{ik\lambda}$$

$$\mathcal{M}_G(k,\lambda) = F_2(k)\,e^{ik\lambda}$$

(2.45)

where

$$F_i(k) = \frac{1}{(f_i)_T}\int_0^1 e^{-ik\xi}\frac{df_i(\xi)}{d\xi}\,d\xi$$

(2.46a)

$$F_2(k) = \frac{L}{(f_2)_T} \int_0^l e^{-ik\xi}(\xi_{ca} - \xi) \frac{df_1(\xi)}{d\xi} d\xi \tag{2.46b}$$

The displacements ζ and θ will also be periodic and may be written as

$$\zeta = \zeta_0 e^{i\omega t} = \zeta_0 e^{ik\xi}$$

$$\theta = \theta_0 e^{i\omega t} = \theta_0 e^{ik\xi} \tag{2.47}$$

where ζ_0 and θ_0 are the amplitude of the displacements and are complex quantities. Substituting Eqs. (2.47) and (2.45) in Eqs. (2.31), the equations of motion in matrix notation become

$$\begin{bmatrix} -\frac{k^2}{\lambda} + ik & -1 - i(m_1 + m_{1,1})k \\ ik & -1 - \frac{k^2}{\mu} - im_2 k \end{bmatrix} \begin{bmatrix} \zeta_0 \\ \theta_0 \end{bmatrix} = \frac{w_0}{V_0} \begin{bmatrix} F_1(k) \\ F_2(k) \end{bmatrix} \tag{2.48}$$

The transfer functions with respect to the vertical and pitch accelerations are obtained from Eqs. (2.48) through the following relationships

$$H_z'' = \frac{\bar{z}_0''}{\bar{w}_0} = -k^2 \frac{\bar{z}_0}{\bar{w}_0}$$

$$H_\theta'' = \frac{\bar{\theta}_0''}{\bar{w}_0} = -k^2 \frac{\bar{\theta}_0}{\bar{w}_0} \qquad (2.49)$$

Finally, the mean square values of these accelerations are found by applying Eq. (2.40)

$$\overline{\ddot{z}^2} = \frac{\overline{w_e^2}}{\pi} \int_0^\infty \left| \frac{\bar{z}_0''}{\bar{w}_0} \right|^2 \frac{(\alpha^2 + 3k^2)\alpha}{(\alpha^2 + k^2)^2} \, dk$$

$$\overline{\ddot{\theta}^2} = \frac{\overline{w_\theta^2}}{\pi} \int_0^\infty \left| \frac{\bar{\theta}_0''}{\bar{w}_0} \right|^2 \frac{(\alpha^2 + 3k^2)\alpha}{(\alpha^2 + k^2)^2} \, dk \qquad (2.50)$$

CHAPTER III

STRUCTURAL LOADS

3.1 Bending Moment and Shear Due to Discrete Gust Excitation

The structural loads acting on the airship may be found by considering the inertia loading and the forces due to gust and motion when the airship is disturbed from its equilibrium flight condition. The airship is assumed to act as a free-free beam with its loading $p(x, t)$ distributed along its longitudinal axis. With reference to the loading diagram given in Figure 2, the shear and bending moment at station X_o are

$$S = \int_0^{x_o} p(x,t)\, dx$$

$$BM = \int_0^{x_o} (x_o - x)\, p(x,t)\, dx \tag{3.1}$$

Substituting $p(x, t)$ from Eq. (2.3), Eqs. (3.1) become

$$S = \int_0^{x_o} \left\{ \frac{dL_G}{dx} + \frac{dL_M}{dx} - m(x)\left[\ddot{h} + (x_{CG} - x)\ddot{\theta}\right] \right\} dx \tag{3.2}$$

$$BM = \int_0^{x_o} (x_o - x) \left\{ \frac{dL_G}{dx} + \frac{dL_M}{dx} - m(x)\left[\ddot{h} + (x_{CG} - x)\ddot{\theta}\right] \right\} dx \tag{3.3}$$

The bending moment may be expressed in nondimensional form by the following coefficient which is commonly used in airship design (Ref. 14).

$$C_{BM} = \frac{BM}{\rho L_a (Vol)^{2/3}} \tag{3.4}$$

Substituting Eqs. (2.9) and (2.23) into Eq. (3.3) and converting to the nondimensional variables λ and ξ, the bending moment coefficient at station ξ_0 due to a gust profile $\frac{W_G}{W_0}(\lambda)$ becomes

$$C_{BM} = \frac{2}{(Vol)^{2/3}} \frac{W_0}{V_0} \left[\int_0^{\lambda} \frac{d}{d\sigma} \left[\frac{W_G(\sigma)}{W_0} \right] \varphi_{BM_{G0}}(\lambda - \sigma)\, d\sigma \right.$$

$$+ \left(\frac{\theta - \xi'}{W_0/V_0} \right) I_1 + \frac{\theta'}{W_0/V_0} I_2 - \frac{\theta''}{W_0/V_0} \left(I_3 + \frac{I_6}{\rho} \right)$$

$$\left. - \frac{\xi''}{W_0/V_0} \left(I_4 + \frac{I_5}{\rho} \right) + \frac{W_G(0)}{W_0} \varphi_{BM_{G0}}(\lambda) \right] \tag{3.5}$$

where $\varphi_{BM_{G0}}$ is the indicial function for bending moment

$$\varphi_{BM_{G0}}(\lambda) = \int_0^{\lambda} (\xi_0 - \xi) \frac{df_1(\xi)}{d\xi}\, d\xi \qquad 0 \le \lambda \le \xi_0$$

$$\varphi_{BM_{G0}}(\lambda) = \int_0^{\xi_0} (\xi_0 - \xi) \frac{df_1(\xi)}{d\xi}\, d\xi \qquad \lambda \ge \xi_0 \tag{3.6}$$

and

$$I_1 = \int_0^{\xi_0} f_1(\xi)\, d\xi$$

$$I_2 = \int_0^{\xi_0} (\xi_0 - \xi_{CG})\, f_1(\xi)\, d\xi$$

$$I_3 = \int_0^{\xi_0} (\xi - \xi_0)(\xi - \xi_{CG})\, f_1(\xi)\, d\xi$$

$$I_4 = \int_0^{\xi_0} (\xi_0 - \xi)\, f_1(\xi)\, d\xi$$

$$I_5 = \int_0^{\xi_0} (\xi_0 - \xi)\, m(\xi)\, d\xi$$

$$I_6 = \int_0^{\xi_0} (\xi - \xi_0)(\xi - \xi_{CG})\, m(\xi)\, d\xi$$

(3.7)

The shear may also be presented in coefficient form by defining a shear coefficient as

$$C_S = \frac{S}{\rho\, (Vol)^{2/3}} \qquad (3.8)$$

Therefore at station $\bar{\xi}_0$, the shear coefficient is

$$C_S = \frac{\rho}{(V_0 t)^{3/8}} \frac{W_0}{V_0} \left[\int_0^{\lambda} \frac{d'}{d\sigma} \left[\frac{W_G(\sigma)}{W_0} \right] \varphi_{SG_0}(\lambda - \sigma)\, d\sigma \right.$$

$$+ \left(\frac{\theta - \xi'}{W_0/V_0} \right) I_{10} + \frac{\theta'}{W_0/V_0} I_{11} - \frac{\xi''}{W_0/V_0} \left(I_1 + \frac{I_7}{\rho} \right)$$

$$\left. - \frac{\theta''}{W_0/V_0} \left(I_9 + \frac{I_8}{\rho} \right) + \frac{W_G(0)}{W_0} \varphi_{SG_0}(\lambda) \right] \tag{3.9}$$

where φ_{SG0} is the indicial function for shear

$$\varphi_{SG0} = f_1(\lambda) \qquad 0 \le \lambda \le \bar{\xi}_0$$

$$\varphi_{SG0} = f_1(\bar{\xi}_0) \qquad \lambda > \bar{\xi}_0 \tag{3.10}$$

and

$$I_7 = \int_0^{\bar{\xi}_0} m(\xi)\, d\xi$$

$$I_8 = \int_0^{\bar{\xi}_0} (\bar{\xi}_{CG} - \xi)\, m(\xi)\, d\xi$$

$$I_9 = \int_0^{\bar{\xi}_0} (\bar{\xi}_{CG} - \xi)\, f_1(\xi)\, d\xi$$

$$I_{10} = f_1(\bar{\xi}_0)$$

$$I_{11} = (\bar{\xi}_0 - \bar{\xi}_{CG})\, f_1(\bar{\xi}_0) + \bar{I}_1$$

(3.11)

3.2 Shear and Bending Moment Due to Random Gust Excitation

The application of generalized harmonic analysis enables one to find the mean square values of the shear and bending moment as functions of the scale of turbulence. The procedure entails first the determination of the transfer functions with respect to shear and bending moment and then the application of Eq. (2.40) to obtain the mean square values.

The transfer function with respect to shear is found by specifying the gust pattern as

$$\frac{w_\sigma}{w_0} = e^{ik(s-\xi)} \tag{3.12}$$

in Eq. (2.23) and the displacements ζ and θ as

$$\zeta = \zeta_0 e^{ikst}$$

$$\theta = \quad e^{ikst} \tag{3.13}$$

in Eqs. (3.9). The resulting steady-state shear expression at station ξ_0 becomes

$$S = 2q \frac{w_0}{V_0} \left\{ \int_0^{\xi_0} e^{-ik\xi} \frac{df_1(\xi)}{d\xi}\, d\xi + \frac{\zeta_0}{w_0/V_0}\left[k^2\left(I_1 + \frac{I_7}{\rho}\right) - ik\, I_{10}\right] + \frac{\theta_0}{w_0/V_0}\left[I_{10} + k^2\left(I_9 + \frac{I_8}{\rho}\right) + ik\, I_{11}\right] \right\} e^{ikst} \tag{3.14}$$

Therefore, rewriting Eq. (3.14) as

$$S = S_0 e^{i\Omega s} \tag{3.15}$$

where

$$S_0 = 2g \frac{W_0}{V_0} \left[S_R + i S_{IM} \right] \tag{3.16}$$

the transfer function with respect to the shear coefficient is

$$H_{C_S} = \frac{S_0/W_0}{g\,(Vol)^{2/3}} = \frac{2}{V_0\,(Vol)^{2/3}} \left[S_R + i S_{IM} \right] \tag{3.17}$$

The expressions S_R and S_{IM} are the real and imaginary components of the terms in the brackets of Eq. (3.14) and are given in Appendix A.

Applying Eq. (2.40), the mean square value of the shear coefficient at station ξ_0 is

$$\overline{C_S^2} = \frac{4}{\pi\,(Vol)^{4/3}} \frac{\overline{W_0^2}}{V_0^2} \int_0^\infty \frac{\left[S_R^2 + S_{IM}^2 \right] (\lambda^2 + 3\Omega^2)}{(\lambda^2 + \Omega^2)^2} \lambda \, d\Omega \tag{3.18}$$

In a similar manner, the steady state amplitude of the bending moment is found to be

$$(BM)_o = 2\rho L \frac{W_o}{V_o} \left\{ \int_0^{\bar{s}_o} (\bar{s}_o - \bar{s}) e^{-ik\bar{s}} \frac{df_i(\bar{s})}{d\bar{s}} d\bar{s} \right.$$

$$+ \frac{\bar{s}_o}{W_o/V_o} \left[k^2 \left(I_4 + \frac{I_5}{\rho} \right) - ik I_1 \right]$$

$$\left. + \frac{\theta_o}{ikb/V_o} \left[I_1 + k^2 \left(I_3 + \frac{I_1}{\rho} \right) + ik I_2 \right] \right\} \qquad (3.19)$$

Rewriting Eq. (3.19) as

$$(BM)_o = 2\rho L_a \frac{W_o}{V_o} \left[(BM)_R + i (BM)_{iM} \right] \qquad (3.20)$$

the transfer function with respect to the bending moment coefficient is

$$H_{BM} = \frac{(BM)_o / W_o}{\rho L_a (VoL)^{2/3}} = \frac{2}{V_o (VoL)^{2/3}} \left[(BM)_R + i (BM)_{iM} \right] \qquad (3.21)$$

and the mean square value is

$$\overline{C_{BM}^2} = \frac{4}{\pi (VoL)^{4/3}} \frac{\overline{w/\alpha}^2}{V_o^2} \int_0^\infty \left[(BM)_R^2 + (BM)_{iM}^2 \right] \frac{(\lambda^2 + 3k^2)/\lambda}{(\lambda^2 + k^2)^2} dk \qquad (3.22)$$

The expressions for $(BM)_R$ and $(BM)_{iM}$ are given in Appendix A.

3.3 Corrections to Account for Viscous Effects

The expressions for the shear and bending moment coefficients, Eqs. (3.9), (3.5), (3.18) and (3.22), are consistent with the loading used to derive the equations of motion (Eq. (2.31)], if the stability derivatives and apparent mass terms of Eqs. (2.31) are derived from slender-body theory and do not include the modifications suggested in Section 2.2 to account for viscous effects. If viscous corrections are included in the equations of motion they should also be included in the shear and bending moment expressions. A means of doing this is to multiply the appropriate terms of the shear and bending moment equations by the ratio of the empirical value to the slender-body value. These corrections are easily introduced since they may be applied directly to the integrals $I_I - I_{II}$, the indicial functions $\varphi_{s_{40}}$, $\varphi_{om_{60}}$, and the functions a_o, β_o of Eqs. (A.14) and γ_o, δ_o, of Eqs. (A.16). Table II presents a tabulation of suggested corrections to the corresponding slender body values which have been applied to the example airship of the next chapter and may also be used for other airships of similar design.

CHAPTER IV

DYNAMIC RESPONSE AND STRUCTURAL LOADS OF A TYPICAL AIRSHIP

The dynamic response and resulting structural loads are computed for a typical non-rigid airship under the influence of discrete and random gust excitations at an altitude of 5,000 feet. The parameters required for the equations of motion are

$$\begin{aligned} \lambda &= .6434 & r_2 &= -3.318 \\ \mu &= 4.114 & m &= .7362 \\ r_1 &= 1.776 & n &= .2923 \end{aligned} \tag{4.1}$$

and were evaluated from the data presented in Table III. It is seen that the variations in these parameters are very small for the four major types of non-rigid airships currently in operation. (Table IV). Furthermore, since the operational altitude of the airship is probably between sea level and 10,000 feet, variations in the air density will also be small. Thus the parameters in Eq. (4.1) above and an altitude of 5,000 feet will be considered as typical of all current non-rigid airships. Therefore, a parametric study will be confined to varying the gust disturbance parameters. The data for Tables III and IV were taken from Refs. 16 and 27.

4.1 Response to Discrete Gust Excitation

The transient response of the example airship is obtained by solving Eqs. (2.31) with the prescribed initial conditions of Eqs. (2.39).

The analysis entails first the determination of the sharp-edged gust functions, Eqs (2.34) and (2.36), the specifications of a gust profile $w_G(s)/w_0$ and the evaluation of $\varphi_{L_G}(s)$ and $\varphi_{M_G}(s)$ from Eqs. (2.37) and (2.38).

The growths of lift and moment due to a sharp-edged gust depend on the apparent area of the cross-section of the airship at the gust front. For sections on the envelope between the bow and fins, $0 \leq \xi \leq \xi_F$, the apparent area is the area of the cross-section

$$f_1(\xi) = \pi R^2 \qquad 0 \leq \xi \leq \xi_F \tag{4.2}$$

where R is the radius of the envelope. For the tail fin configuration of Figure 4a the apparent area of each cross-section is (Ref. 24)

$$f_1(\xi) = \pi R^2 \left[\frac{S_F^2}{R^2} \cdot \frac{R^2}{S_F^2} - 1 \right] \tag{4.3}$$

The fins of the example airship also have a cruciform configuration but are at 45 degrees with the vertical plane, as shown in Figure 3b. Since the fins are rotated at 45 degrees, the vertical lift of the cross-section shown in Figure 3a is identical to that shown in Figure 3b if both are immersed in the same flow. Hence, Eq. (4.3) will be used in this report. The expression for the envelope radius R was obtained from Ref. 25

$$R(\xi) = 2 R_{MAX} (1.1911 - .4252\xi)\sqrt{\xi(1-\xi)} \tag{4.4}$$

Using Eq. (4.4), the indicial functions for lift and moment due to gust penetration, Eqs. (2.34) and (2.36), are

$$\varphi_{L_{GO}} = \frac{4\pi R_N^2}{(f_1)_T}\left[1.4187\Delta - 2.4317\Delta^2 + 1.1938\Delta^3 - .1808\Delta^4\right] \qquad (4.5)$$

$$\varphi_{M_{GO}} = \frac{4\pi R_N^2 L}{(f_2)_T}\left[.64830\Delta - 1.8206\Delta^2 + 2.1667\Delta^3 - .9780\Delta^4 + .1446\Delta^5\right] \qquad 0 \le \Delta \le \bar{\xi}_F \qquad (4.6)$$

where

$$(f_1)_T = 4200 \ FT^2$$

$$(f_2)_T = 3757 \times 10^2 \ FT^3 \qquad (4.7)$$

For cross-sections on the fin body combination, $\bar{\xi}_F \le \bar{\xi} \le \bar{\xi}_T$. Eq. (4.3) was evaluated from Figure 4 which presents the approximate planform of the example airship fin. The apparent area in this region was approximated by straight line segments as shown in Figure 5 and the indicial functions for this region are

$$\varphi_{L_{GO}(\Delta)} = \frac{1900 + 46131(\Delta - \bar{\xi}_F)}{(f_1)_T} \qquad \bar{\xi}_F \le \Delta \le \bar{\xi}_T$$

$$\varphi_{LG0}(\lambda) = \frac{3720 + 6259(\lambda - \xi_T)}{(f_1)_T} \qquad \xi_{\tilde{m}} \le \lambda \le \xi_T$$

$$\varphi_{LG0}(\lambda) = 1.0 \qquad \lambda \ge \xi_1$$

(4.8)

and

$$\varphi_{MG0}(\lambda) = \frac{4\times10^3}{(f_2)_T}\left[.38202 + 18.805\lambda - 20.566\lambda^2\right] \qquad \xi_{\tilde{m}} \le \lambda \le \xi_T$$

$$\varphi_{MG0}(\lambda) = \frac{4\times10^3}{(f_2)_T}\left[1.1777 + 2.8614\lambda - 3.1295\lambda^2\right] \qquad \xi_{\tilde{m}} \le \lambda \le \xi_T$$

$$\varphi_{MG0}(\lambda) = 1.0 \qquad \lambda \ge \xi_T$$

(4.9)

where

$$\xi = .8171$$
$$\xi_{\tilde{m}} = .8614$$
$$\xi_T = .9381$$
$$\xi_{CG} = .4572$$

(4.10)

Plots of φ_{LG0} and φ_{MG0} are presented in Figure 6.

The discrete gust profile selected for this study is

$$\frac{W_G}{W_0}(s) = \frac{1}{2}\left[1 - \cos \pi \frac{s}{s_G}\right] \qquad 0 \le s \le 2 s_G$$

$$\frac{W_G}{W_0}(s) = 0 \qquad s > 2 s_G \tag{4.11}$$

where s_G is the gust gradient distance in terms of the airship length. Plots of the growths of lift and moment due to this profile were obtained by numerical integration of Eqs. (2.37) and (2.38) and are presented in Figures 7 and 8 for values of s_G equal to 1/12, 1/6, 1/3, 1/2, 3/4.

The equations of motion were solved numerically by using an Adam's method expansion retaining third differences. The required first four points of the expansion were obtained by a Runge-Kutta solution of the two differential equations of motion. This numerical procedure is commonly used in solving equations of this nature and may be found in a standard text such as Ref. 26. The computations were performed on the Burroughs E-101 Digital Computer.

A typical time history of the nondimensional response of the airship to a one-minus-cosine gust with a gradient distance $s_G = 1/2$ is presented in Figures 9 and 10. This gradient distance was selected as an illustration because it produces the critical loading on the airship. This is discussed in the next chapter. The results of the transient response are summarized in Figure 11, which presents the maximum values of the nondimensional vertical and pitching accelerations of the center of gravity as functions of the parameter s_G. The times for these accelerations to reach their peak values are also presented and given in terms of the penetration distance s.

Time histories of the following have also been calculated as a function of the parameter Δ_2 :

a. Figure 12. The angle of attack at the center of pressure of the fin (ξ_{cp} = .8543) calculated from

$$\frac{\alpha(\Delta)}{W_0/V_0} = \frac{\theta}{W_0/V_0} - \frac{\zeta'}{W_0/V_0} + (\xi_{cp} - \xi_{cg})\frac{\theta'}{W_0/V_0} \qquad 0 \le \Delta \le \xi_{cp}$$

$$\frac{\alpha(\Delta)}{W_0/V_0} = \frac{\theta}{W_0/V_0} - \frac{\zeta'}{W_0/V_0} + (\xi_{cp} - \xi_{cg})\frac{\theta'}{W_0/V_0} + \frac{1}{2}\left[1 - \cos\pi\frac{(\Delta - \xi_{cp})}{\Delta_2}\right] \qquad \Delta > \xi_{cp} \tag{4.12}$$

b. Figure 13. The non-dimensional vertical acceleration of the tail section at the center of pressure of the fin, calculated from

$$\frac{\zeta_T''}{W_0/V_0} = \frac{\zeta''}{W_0/V_0} - (\xi_{cp} - \xi_{cg})\frac{\theta''}{W_0/V_0} \tag{4.13}$$

4.2 Response to Random Gust Excitation

The procedure in the random gust analysis requires first the determination of the steady-state lift and moment functions, $F_1(k)$ and $F_2(k)$, given by Eqs. (2.46) and the computation of the transfer functions H_L'' and H_θ'', Eqs. (2.49). Plots of the absolute values of $|F_1(k)|$, $|F_2(k)|$, $|H_\xi''|^2$, and $|H_\theta''|^2$ are given in Figures 14 through 17 as functions of the reduced frequency k. The mean square values $\overline{\xi''^2}$ and $\overline{\theta''^2}$ are presented in Figure 18 as functions of the scale of turbulence $\mathcal{L}$, obtained by numerical integration of Eq. (2.50). The integrals were found to converge at k = 100. The power spectral density of the disturbance used for the computations, Eq. (2.43), is presented in Figures 19 for values of the scale of turbulence ranging from 100 to 2000 feet.

4.3 Structural Loads Due to Discrete Gust Excitation

The physical and apparent mass data required for the structural analysis is presented in Table V for various stations $\bar{\xi}_o$ along the longitudinal axis of the airship. The distributed mass of the example airship was taken from Ref. 16 and is presented in Figure 20.

A time history of the shear coefficient, Eq. (3.9), at station $\bar{\xi}_o = .8171$, is presented in Figure 21 as a function of s_G. At this station the shear represents the normal load on the tail section and is of primary importance in design work. A time history of the bending moment coefficient, Eq. (3.5), was computed at $\bar{\xi}_o = .4572$ where it was anticipated to be a maximum and is presented in Figure 22. The maximum value of C_{BM} is very important to the designer since it dictates to a large extent the design of the airship envelope.

The following computations are also presented:

a. Figure 23. Peak values of $C_{BM}/W_o N_o$ at $\bar{\xi}_o = .4572$ and $C_S/W_o N_o$ at $\bar{\xi}_o = .8171$ as a function of s_G.

b. Figures 24 and 25. Time histories of $C_s/w_o/V_o$ at $\bar{s}_o = .3171$ and $C_{BM}/w_o/V_o$ at $\bar{s}_o = .4572$ for $\lambda_o = 1/3$, to illustrate the relative contributions of the disturbance, motion, and inertia forces to the shear and bending moment.

c. Figure 26. First positive peak and first negative peak of $C_s/w_o/V_o$ at stations $\bar{s}_o = .2065, .3540, .5900, .7080, .8171$.

d. Figure 27. Envelope of peak values of $C_{BM}/w_o/V_o$ and times of occurrence.

4.4 Structural Loads Due to Random Gust Excitation

The numerical results of the random gust analysis are summarized in the following figures:

a. Figure 28. Square of absolute value of transfer function with respect to shear coefficient versus k at station $\bar{s}_o = .8171$, calculated from Eq. (3.17).

b. Figure 29. Square of absolute value of transfer function with respect to bending moment coefficient versus k at station $\bar{s}_o = .4572$, calculated from Eq. (3.21).

c. Figure 30. Mean square values of shear and bending moment coefficients versus scale of turbulence, calculated by numerical integration of Eqs. (3.18) and (3.27).

CHAPTER V

DISCUSSION AND CONCLUSIONS

5.1 Discussion of Calculated Results

In the previous chapter the responses and structural loads of the example airship experiencing a one-minus-cosine gust and random gust disturbances have been calculated. They are presented in nondimensional form independent of the gust amplitude W_o and the forward velocity of the airship V_o. As indicated in Chapter IV, these results also represent approximately the characteristics of other non-rigid airships currently in operation.

The significant observations that may be made from Figure 11 are that the pitching acceleration reaches a critical value for a gust with a gradient distance of approximately 1/4 whereas the vertical acceleration is critical for a gradient distance of approximately 3/4. In both cases the peak accelerations occur shortly after the gust peak. The results of the random gust analysis (Figure 18) indicate that a scale of turbulence of approximately 1-1/2 airship lengths is critical for the vertical acceleration. Though there is insufficient information in Figure 18 to determine a critical scale of turbulence for the pitching acceleration, it appears to be less than 1/2 an airship length. Correlation between the discrete and random gust results is favorable. Both analyses show that the critical wave length of atmospheric disturbance is shorter for the pitching acceleration than for the vertical acceleration. Also, the values of $-\left[\bar{\ddot{z}}/w_g\right]_{max}$ and $\left[\bar{\ddot{z}}/\dot{w}_g/V\right]_{max}$ agree very well, the ratio of the former to the latter being 1.5 to 1.3. It should be noted that this last result is to be expected and is discussed further in Ref. 22 in which the discrete and random gust alleviation factors of a rigid airplane were also comparable.

The results of the structural load analysis are even more significant since the designer is primarily interested in the maximum bending moment on the envelope and the maximum load on the tail section. The results in

Figures 22, 23 and 27 show that the maximum bending moment on the envelope occurs very near the location of the center of gravity of the airship ($\xi_o = .45$) and is caused by a gust of approximately one airship length ($\Delta_G = 1/2$). Figure 23 indicates that in each case the peak of the bending moment at the center of gravity occurs shortly after the gust peak. The normal load at the tail section (the shear at $\xi_o = .8171$) also reaches a critical value for $\Delta_G = 1/2$ (Figures 2' and 23). This critical value is attained at a penetration distance of 1.26 airship lengths or at approximately half an airship length after the gust front strikes the tail fin leading edge. As with the case of the vertical and pitching accelerations, there is also favorable correlation between the discrete and random load analyses. The random analysis (Figure 30) shows that a scale of turbulence of approximately one airship length ($\lambda^2/L = 1$) is critical for both the maximum envelope bending moment and the tail load. Therefore, both methods of analysis indicate that the critical wave length of atmospheric turbulence is the same for the envelope and tail loadings. The maximum values of the curves of Figures 23 and 30 compare as follows:

$$\left(\frac{C_{BM}}{W_o/V_o}\right)_{MAX} = .0805$$

$$\left(\frac{\bar{C}_{BM}}{\bar{W}_G/V_o}\right)_{MAX} = .0866$$

$$\left(\frac{C_S}{W_o/V_o}\right)_{MAX} = -.295$$

$$\left(\frac{\bar{C}_S}{\bar{W}_G/V_o}\right)_{MAX} = \pm .336 \qquad (5.1)$$

The results of this section indicate that to determine a critical gust length for the airship it is necessary to go beyond the determination of the response of the airship, i.e., it is necessary to calculate the loads on the

airship. This point is supported by the fact that the critical values of the vertical acceleration of the center of gravity and the pitching acceleration are not caused by the same gust length which results in critical values for the loading ($\mathcal{L}_g = 1/2$). Furthermore, the angle of attack at the center of pressure of the fin (Figure 12) indicates that $\mathcal{L}_g = 1/12$ is critical whereas the vertical acceleration at this station (Figure 13) indicates that an $\mathcal{L}_g$ of 3/4 or perhaps greater may be critical. Therefore, on the basis of the structural load analysis it is concluded that the critical length of a one-minus-cosine gust and the critical scale of turbulence are both approximately one airship length and that Figure 23 could form the basis of a gust design criterion. These results do not agree with Flomenhoft's conclusion (Ref. 15) that a gust with a length of three fin chords is critical. It is realized that his conclusions are based on the acceleration response of the tail instead of the loading.

5.2 Comparison with Sharp-Edged Gust Results

A comparison will be made with the procedure followed in Refs. 16 and 17 in which the loads on the airship are analyzed for a 30 foot per second sharp-edged gust applied normal to the plane of the tail fins. The shear and bending moment distributions are computed based on the vertical load at the stern due to this sharp-edged gust. This procedure does not consider gust loading of the envelope and presumes that this stern load represents the most critical gust loading condition. The results of the present investigation, however, (Figure 22), show that the maximum bending moment occurs before the one-minus-cosine gust reaches the fin leading edge (at $\mathcal{L} = .57$). To show that the maximum tail load as computed by the method of this report does not result in the critical bending moment on the envelope and that the envelope loading is important, the following calculations are made. Assuming that W_o, the peak of the one-minus-cosine gust, is 30 feet per second and V_o, the forward velocity is 122 feet per second, the maximum upward tail load is found from Eq. (5.1) to be

$$P_T = -S_{MAX} = (C_S)_{MAX} (V_{TL})^{2/3} \frac{\rho}{g} = 10,900 \text{ lbs} \tag{5.2}$$

The moment due to this load about the center of gravity is 1,440,000 ft-lbs. The net load contributed by the distributed loading on the envelope between the center of gravity and the tail fins, calculated at the instant that the tail load is a maximum, was found to be 14,620 lbs. downward. As a result the net bending moment about the center of gravity becomes only approximately 200,000 ft-lb. It is seen that this number is a small difference between two large numbers and its accuracy depends on the accuracy of the distributed loading on the rear half of the envelope. This distributed loading is essentially the loading due to the gust disturbance which itself requires experimental verification. One way to accomplish this is to record the time history of the bending moment at the center of gravity and to verify the fact that the gust disturbance at the tail will cause very high local shear but a small bending moment at the center of gravity station of the airship.

A further comparison may be made of the maximum bending moment on the envelope and the shear at the tail section. Reference 16 gives

$$(BM)_{MAX} = 840,000 \text{ FT-LBS}$$

$$S = -10,000 \text{ lbs} \tag{5.3}$$

and the results of the present investigation give

$$(BM)_{MAX} = 1,010,000 \text{ FT-LBS}$$

$$S_{MAX} = -10,900 \text{ lbs} \tag{5.4}$$

The results of Ref. 16 then are unconservative in comparison with the present investigation, moreso for the bending moment than for the shear.

In calculating the operating pressure of the envelope, the value of $(C_{BM})_{MAX}$ that is commonly used is .018 (Ref. 16) and is independent of the gust amplitude and the airship flight velocity. The value of $(C_{BM})_{MAX}$ obtained from Eq. (5.1), however, is a function of both the gust amplitude and the flight speed. For a gust amplitude of 30 feet per second and a flight speed of 122 feet per second, Eq. (5.1) gives a value of .0198.

5.3 Conclusions

The major conclusions of this report may be summarized as follows:

1. There is no appreciable difference between the discrete gust factors $\left(\bar{F}''_{W_G/U_e}\right)_{MAX}$, $\left(\bar{C}_S/N_0/U_e\right)_{MAX}$ and $\left(\bar{C}_{BM}/N_0/V_e\right)_{MAX}$ and the random gust factors $\left(\bar{F}''_{W_G/U_e}\right)_{MAX}$ $\left(\bar{C}_S/W_G/V_e\right)_{MAX}$ and $\left(\bar{C}_{BM}/W_G/V_e\right)_{MAX}$

2. One-minus-cosine gusts of one airship length and random gust disturbances with a scale of turbulence of one airship length are critical for both the envelope and empennage loading of the airship.

3. Gust loads on the envelope are important and should be considered in a theoretical analysis.

4. The critical gust load parameters for the envelope and empennage of non-rigid airships currently in operation, based on the discrete gust analysis, are

$$C_{BM} = .081 \frac{W_0}{V_0}$$

$$C_S = -.30 \frac{W_0}{V_0}$$

5.4 Recommendations for Future Research

It is recommended that the example airship be instrumented for flight testing to obtain comparison with the theoretical results of this report. For correlation with the discrete gust study, time histories of the following should be recorded:

1. Vertical velocity and acceleration of the center of gravity,
2. Pitching angle, velocity, and acceleration,
3. Vertical acceleration of the tail section,
4. Normal load on the empennage and bending moment at the center of gravity of the airship.

For a correlation with the theoretical random gust study, the transfer functions of the vertical and pitching accelerations and of the empennage load and envelope bending moment should be obtained. During the test runs the controls of the airship should be locked and any deviations from a prescribed setting should be recorded. The NACA and the Boeing Airplane Company have been successful in conducting similar tests for airplanes and Refs. 28, 29 and 30 are recommended for further study. Two basic methods which have been used by the NACA (Ref. 28) to determine the amplitudes of the transfer functions may be mentioned. The first method makes use of the power spectrums of the airplane response and the gust input. The second method requires the spectrum of airplane response and the cross spectrum between the gust input and the airplane response. If the measurements of the gust input are accurate, the two methods should give identical results. In determining a means by which the gust input could be measured, consideration should be given to the feasibility of using a flow-direction vane mounted on a boom and attached to the bow of the airship. Serious boom vibrational problems may arise, since the boom must be long enough so that the vane measurements can be made out of the airship flow field. If this method is not successful, the method suggested in Ref. 15 may be tried in which an instrumented airplane would record the turbulence level in the neighborhood of the airship by making successive

passes by the airship. This latter method is feasible for measurements of the power spectrum of the gust but not applicable for measurements of the cross spectrum between the gust and airship response.

It is realized that the controls locked condition is somewhat idealistic and that the pilot is constantly using the controls to correct for disturbances. It is suggested, therefore, that a theoretical study be made which will include an automatic control system and will consider the effects of control surface deflections on the response and loading of the airship.

APPENDIX A

TRANSFER FUNCTIONS OF THE EXAMPLE AIRSHIP

A.1 Vertical and Pitching Accelerations

The transfer functions with respect to the vertical and pitching accelerations of the airship are found by applying Cramer's rule to the system of Eqs. (2.48):

$$\frac{\zeta_0}{w_0} = \frac{1}{V_0} \frac{\begin{vmatrix} F_1(k) & -1 - i(m + m\lambda_1)k \\ F_2(k) & -1 - \frac{k^2}{\mu} - i m\lambda_2 k \end{vmatrix}}{\Delta(k)} \tag{A.1}$$

$$\frac{\theta_0}{w_0} = \frac{1}{V_0} \frac{\begin{vmatrix} -\frac{k^2}{\lambda} + ik & F_1(k) \\ -ik & F_2(k) \end{vmatrix}}{\Delta(k)} \tag{A.2}$$

where

$$\Delta(k) = \begin{vmatrix} -\frac{k^2}{\lambda} + ik & -1 - i(m + m\lambda_1)k \\ ik & -1 - \frac{k^2}{\mu} - i m\lambda_2 k \end{vmatrix} \tag{A.3}$$

The lift and moment functions $F_1(k)$ and $F_2(k)$ are

$$F_1(A) = \frac{1}{(f_1)_T}\int_0^1 e^{-cA\xi}\frac{df_1(\xi)}{d\xi}\,d\xi$$

$$F_2(A) = \frac{L_a}{(f_2)_T}\int_0^1 e^{-cA\xi}(\xi_{c.g.}-\xi)\frac{df_1(\xi)}{d\xi}\,d\xi$$

(2.46)

where the apparent area $f_1(\xi)$ is

$$f_1(\xi) = 4\pi R_M^2\left(a_1\xi - \frac{a_2}{2}\xi^2 + \frac{a_3}{3}\xi^3 - \frac{a_4}{4}\xi^4\right) \qquad 0 \le \xi \le \xi_F$$

$$f_1(\xi) = 1900 + 41{,}131\,(\xi - \xi_F) \qquad \xi_F \le \xi \le \xi_M$$

$$f_1(\xi) = 3720 + 6259\,(\xi - \xi_T) \qquad \xi_M \le \xi \le \xi_T$$

$$f_1(\xi) = (f_1)_T = 4200\ FT^2 \qquad \xi_T \le \xi \le 1.0$$

(A.4)

and

$$a_1 = 1.4187$$
$$a_2 = 4.8634$$
$$a_3 = 3.5814$$
$$a_4 = 0.7232 \qquad \text{(A.5)}$$

Substituting Eqs. (A.4) into Eqs. (2.46) and integrating, $F_1(k)$ and $F_2(k)$ can be reduced to the following forms:

$$F_1(k) = \frac{1}{k}\frac{4\pi R_M^2}{(f_1)_T}\Big[(A_1 \sin k\bar{\xi}_F + A_2 \cos k\bar{\xi}_F + A_3 \sin k\bar{\xi}_M + A_4 \sin k\bar{\xi}_T + A_5) + i(A_1 \cos k\bar{\xi}_F - A_2 \sin k\bar{\xi}_F + A_3 \cos k\bar{\xi}_M + A_4 \cos k\bar{\xi}_T + A_6)\Big] \qquad \text{(A.6)}$$

$$F_2(k) = \frac{L_a}{k}\frac{4\pi R_M^2}{(f_2)_T}\Big[(B_1 \sin k\bar{\xi}_F + B_2 \cos k\bar{\xi}_F - B_3 \cos k\bar{\xi}_M + B_4 \sin k\bar{\xi}_M - B_5 \cos k\bar{\xi}_T + B_6 \sin k\bar{\xi}_T + B_7) + i(B_1 \cos k\bar{\xi}_F - B_2 \sin k\bar{\xi}_F + B_3 \sin k\bar{\xi}_M + B_4 \cos k\bar{\xi}_M + B_5 \sin k\bar{\xi}_T + B_6 \cos k\bar{\xi}_T + B_8)\Big] \qquad \text{(A.7)}$$

where

$$A_1 = a_1 - a_2 \xi_F + a_3 \xi_F^2 - a_4 \xi_F^3 + \frac{2(3a_4 \xi_F - a_3)}{k^2} - \frac{41,131}{4\pi R_M^2}$$

$$A_2 = \frac{-a_2 + 2a_3 \xi_F - 3a_4 \xi_F^2}{k} + \frac{6a_4}{k^3}$$

$$A_3 = \frac{34,872}{4\pi R_M^4}$$

$$A_4 = \frac{6259}{4\pi R_M^4}$$

$$A_5 = \frac{a_2}{k} - \frac{6a_4}{k^3}$$

$$A_6 = \frac{2a_3}{k^2} - a_1$$

$$B_1 = (\xi_{CG} - \xi_F)\left(a_1 - a_2 \xi_F + a_3 \xi_F^2 - a_4 \xi_F^3 - \frac{41,131}{4\pi R_M^2}\right)$$

$$+ \frac{2\left[-a_2 + a_3(3\xi_F - \xi_{CG}) - 3a_4 \xi_F (2\xi_F - \xi_{CG})\right]}{k^2}$$

$$+ 24 \frac{a_4}{k^4}$$

$$B_2 = \frac{-a_1 + a_2(2\bar{\xi}_m - \bar{\xi}_{CG}) + a_3\bar{\xi}_m(2\bar{\xi}_{CG} - 3\bar{\xi}_m) + a_4\bar{\xi}_m^2(4\bar{\xi}_m - 3\bar{\xi}_{CG})}{k}$$

$$+ 6\frac{[a_3 + a_4(\bar{\xi}_{CG} - 4\bar{\xi}_T)]}{k^3} + \frac{41,131}{4\pi R_M^2 k}$$

$$B_3 = \frac{34,872}{4\pi R_M^2 k}$$

$$B_4 = \frac{34,872\,(\bar{\xi}_{CG} \cdot \bar{\xi}_M)}{4\pi R_M^2}$$

$$B_5 = \frac{6259}{4\pi R_M^2 k}$$

$$B_6 = \frac{6259(\bar{\xi}_{CG} - \bar{\xi}_T)}{4\pi R_M^2}$$

$$B_7 = \frac{a_1 + a_2\bar{\xi}_{CG}}{k} - \frac{6(a_3 + a_4\bar{\xi}_{CG})}{k^3}$$

$$B_8 = -a_1\bar{\xi}_{CG} + \frac{2(a_1\bar{\xi}_{CG} + a_2)}{k^2} - \frac{24a_4}{k^4}$$

(A. 8)

The singularities of $F_1(k)$ and $F_2(k)$ at $k = 0$ were investigated by utilizing the series expansions for the sine and cosine terms of Eqs. (A. 6) and (A. 7) about the point $k = 0$. Following this procedure

$$F_1(0) = F_2(0) = 1.0 \tag{A.9}$$

Rewriting $F_1(k)$ and $F_2(k)$ as

$$F_1(k) = F_{1_R} + i F_{1_M}$$

$$F_2(k) = F_{2_R} + i F_{2_M} \tag{A.10}$$

Eqs. (A.1) and (A.2) in expanded form become

$$\frac{\zeta_0}{w_0} = \frac{\lambda\mu}{V_0 k^2}\left[\frac{A_0 + iB_0}{C_0 + iD_0}\right]$$

$$\frac{\theta_0}{w_0} = \frac{\lambda\mu}{V_0 k}\left[\frac{E_0 + iF_0}{C_0 + iD_0}\right] \tag{A.11}$$

where

$$A_0 = -F_{1_R}\left(1 + \frac{k^2}{\mu^2}\right) + k\left[m k_2 F_{1_M} - F_{2_M}(m + m k_1)\right] + F_{2_R}$$

$$B_0 = -F_{1_M}\left(1 + \frac{k^2}{\mu^2}\right) + k\left[F_{2_R}(m + m k_1) - F_{1_R} m k_2\right] + F_{2_M}$$

$$C_0 = k^2 + \mu + i\mu\left[m(\Omega_2 - \Omega_1) - m_1\right]$$

$$D_0 = k\left(\mu m \Omega_2 - \lambda\right)$$

$$E_0 = -\frac{F_{2_R} k}{\lambda} + F_{1_{IM}} - F_{2_{IM}}$$

$$F_0 = -\frac{F_{2_{IM}} k}{\lambda} + F_{2_R} - F_{1_R}$$

(A. 12)

A. 2 Shear and Bending Moment

The real and imaginary components, S_R and S_{IM}, of the steady-state shear coefficient, Eq. (3.17), are obtained from Eq. (3.14) by introducing the displacement amplitudes of Eq. (A.11). For values of ξ_0 between 0 and ξ_F which are of interest in this report:

$$S_R = 4\pi R_M^2 \alpha_0 + \frac{\lambda\mu}{C_0^2 + D_0^2}\left(C_0 S_A + D_0 S_B\right)$$

$$S_{IM} = 4\pi R_M^2 \beta_0 + \frac{\lambda\mu}{C_0^2 + D_0^2}\left(C_0 S_B - D_0 S_A\right)$$

(A. 13)

where

$$\alpha_0 = \alpha_1 \cos k\xi_0 + \beta_1 \sin k\xi_0 + \alpha_2$$

$$\beta_0 = \beta_1 \cos k\xi_0 - \alpha_1 \sin k\xi_0 + \beta_2$$

$$S_A = A_0\left(I_1 + \frac{I_7}{\rho}\right) + \frac{B_0}{k} I_{10} + E_0\left[\frac{I_{10}}{k} + k\left(I_9 + \frac{I_8}{\rho}\right)\right] - F_0 I_{11}$$

$$S_B = -\frac{A_0}{k} I_{10} + B_0\left(I_1 + \frac{I_7}{\rho}\right) + E_0 I_{11} + F_0\left[\frac{I_{10}}{k} + k\left(I_9 + \frac{I_8}{\rho}\right)\right]$$

$$\alpha_1 = \frac{-a_2 + 2a_3\xi_0 - 3a_4\xi_0^2}{k^2} + \frac{6a_4}{k^4}$$

$$\beta_1 = \frac{a_1 - a_2\xi_0 + a_3\xi_0^2 - a_4\xi_0^3}{k} + \frac{2(3a_4\xi_0 - a_3)}{k^3}$$

$$\alpha_2 = \frac{a_2}{k^2} - \frac{6a_4}{k^4}$$

$$\beta_2 = -\frac{a_1}{k} + 2\frac{a_3}{k^3}$$

(A. 14)

Similarly, for the steady-state bending moment coefficient, Eq. (3.21), substituting Eqs. (A.11) into Eq. (3.19) results in the following expressions for the interval $0 \le \xi_0 \le \xi_F$

$$(BM)_R = 4\pi R_M^2 \gamma_0 + \frac{\lambda\mu}{C_0^2+D_0^2}\left[C_0(BM)_A + D_0(BM)_B\right]$$

$$(BM)_{IM} = 4\pi R_M^2 \delta_0 + \frac{\lambda\mu}{C_0^2+D_0^2}\left[C_0(BM)_B - D_0(BM)_A\right] \qquad (A.15)$$

where

$$\gamma_0 = \alpha_4 \cos k\xi_0 + \alpha_5 \sin k\xi_0 + \alpha_6$$

$$\delta_0 = \alpha_5 \cos k\xi_0 - \alpha_4 \sin k\xi_0 + \alpha_7$$

$$(BM)_A = A_0\left(I_4 + \frac{I_2}{\rho}\right) + B_0\frac{I_1}{k} + E_0\left[\frac{I_1}{k} + k\left(I_3 + \frac{I_4}{\rho}\right)\right] - F_0 I_2$$

$$(BM)_B = -A_0\frac{I_1}{k} + B_0\left(I_4 + \frac{I_2}{\rho}\right) + E_0 I_2 + F_0\left[\frac{I_1}{k} + k\left(I_3 + \frac{I_4}{\rho}\right)\right]$$

$$\alpha_4 = \frac{-a_1 + a_2\xi_0 - a_3\xi_0^2 + a_4\xi_0^3}{k^2} + \frac{6(a_3 - 3a_4\xi_0)}{k^4}$$

$$\alpha_5 = \frac{-2a_2 + 4a_3\xi_0 - 6a_4\xi_0^2}{k^3} + \frac{24\,a_4}{k^5}$$

$$\alpha_6 = \frac{a_1 + a_2 \bar{s}_0}{k^2} - \frac{6(a_3 + a_4 \bar{s}_0)}{k^4}$$

$$\alpha_7 = -\frac{a_1 \bar{s}_0}{k} + \frac{2(a_2 + a_3 \bar{s}_0)}{k^3} - \frac{24 \bar{\tau}_y}{k^5} \qquad (A.16)$$

REFERENCES

1. Munk, Max M., The Aerodynamic Forces on Airship Hulls, NACA Report 184, 1924.

2. Ames, Joseph S., A Résumé of the Advances in Theoretical Aeronautics Made by Max M. Munk, NACA Report 213, 1925.

3. Zahm, A. F., Flow and Force Equations for a Body Revolving in a Fluid, NACA Report 323, 1928.

4. Upson, R. H. and Klikoff, W. A., Application of Practical Hydrodynamics to Airship Design, NACA Report 405, 1931.

5. Burgess, C. P., Forces on Airships In Gusts, NACA Report 204, 1924.

6. Arnstein, K. and Klemperer, W., Performance of Airships, Division R of Aerodynamic Theory, Vol. VI, W. F. Durand, Editor-in-Chief, Julius Springer, Berlin, 1936.

7. Special Committee on Airships, Review and Analysis of Airship Design and Construction Past and Present, Report No. 2, Appendix I, Supplement 7, Stanford University Press, January 30, 1937.

8. Harrington, R. P., An Attack on the Origin of Lift of an Elongated Body, Daniel Guggenheim Airship Institute, Publication No. 2, 1935.

9. Kuethe, Arnold M., A Water Tank for Model Tests on the Motion of Airships in Gusts, Journal of the Aeronautical Sciences, Vol. 5, No. 6, April 1938.

10. Allen, H. J. and Perkins, E. W., A Study of Effects of Viscosity on Flow Over Slender Inclined Bodies of Revolution, NACA Report 1048, 1951.

11. Kelly, H. R., The Estimation of Normal-Force, Drag, and Pitching-Moment Coefficients for Blunt-Based Bodies of Revolution at Large Angles of Attack, Journal of Aeronautical Science, Vol. 21, No. 8, August 1954.

12. Hill, Jacques A. F., A Non-Linear Theory of The Lift on Slender Bodies of Revolution, Presented at the U. S. Naval Symposium on Aeroballistics, Laurel, Maryland, 19-20 October 1954.

13. Ashley, H., Zartarian, G., and Neilson, D. O., Investigation of Certain Unsteady Aerodynamic Effects in Longitudinal Dynamic Stability, AF Technical Report 5986, 1951.

14. Foss, Kenneth A., Effects of Structural Flexibility on Gust Loading of Aircraft, Part I - Gust Loads on Swept-Wing Airplanes Free to Pitch and to Deform Statically, WADC TR 54-592, Part I, March 1955.

15. Flomenhoft, H. I., Gust Loads on Airship Fins, McLean Report No. E-114, June 1957.

16. Barton, J. A., et. al., Stress Analysis of GN975C2N Envelope, Goodyear Aircraft Corporation Report No. 5320, November 23, 1953.

17. Bingham, O. K. and Liebert, ' R., Determination of Air loads on Model ZPN Empennage, Model ZP2N-1 Empennage, Model ZP2N-1W Empennage, Goodyear Aircraft Corporation Report No. 1903, April 11, 1950. (Report Confidential)

18. Jones, R. T., Properties of Low-Aspect-Ratio Pointed Wings at Speeds Below and Above the Speed of Sound, NACA TR 835, 1946.

19. Adams, M. C. and Sears, W. R., Slender-Body Theory - Review and Extension, Journal of the Aeronautical Sciences, Vol. 20, No. 2, February 1953.

20. Lawrence, H. R. and Flax, A. H., Wing-Body Interference at Subsonic and Supersonic Speeds - Survey and New Developments, Journal of the Aeronautical Sciences, Vol. 21, No. 5, May 1954.

21. Press, H. and Houbolt, J. C., Some Applications of Generalized Harmonic Analysis to Gust Loads of Airplanes, Journal of the Aeronautical Sciences, Vol. 22, No. 1, January 1955.

22. Bisplinghoff, R. L., Pian, T. H. H., Foss, K. A., Response of Elastic Aircraft to Continuous Turbulence, Presented at the Structures and Materials Panel of the AGARD meeting at Oslo and Copenhagen, April 24 to May 4, 1957.

23. Press, Harry, Atmospheric Turbulence Environment with Special Reference to Continuous Turbulence, Presented to Structures and Materials Panel, AGARD, Copenhagen, Denmark, April 29 - May 4, 1957.

24. Bryson, A. E., Evaluation of the Inertia Coefficients of the Cross Section of a Slender Body, Journal of the Aeronautical Sciences, Readers' Forum, Vol. 21, No. 6, June 1954.

25. Anderson, A. W. and Flickinger, S. J., Jr., Wind-Tunnel Tests of a 1/48-Scale Model of the XZS2G-1 Airship with Various Tail Configurations, Part I - Longitudinal and Drag Characteristics, David W. Taylor Model Basin Report No. 866, September 1954, (Report Confidential).

26. Hildebrand, F. B., Introduction to Numerical Analysis, McGraw-Hill Book Company, Inc., New York, 1956.

27. Letter from Goodyear Aircraft Corporation dated August 2, 1957.

28. Coleman, T. L. and Press H., Effects of Airplane Flexibility on Wing Bending Strains in Rough Air, NACA TN 4055, July 1957.

29. Coleman, T. L., Murrow, H. N., and Press H., Some Structural Response Characteristics of a Large Flexible Swept-Wing Airplane in Rough Air, Institute of Aeronautical Sciences, Preprint, No. 785, January 1958.

30. Jackson, C. E. and Wherry, J. E., A Comparison of Theoretical and Experimental Loads on the B-47 Resulting From Discrete Vertical Gusts, Institute of Aeronautical Sciences, Preprint No. 784 . January 1958.

TABLE I

COMPARISON OF AERODYNAMIC STABILITY DERIVATIVES OF EXAMPLE AIRSHIP

	A	= B	
	Slender Body Value	Semi-Empirical Value	$\frac{B}{A}$
$\partial C_L / \partial \alpha$	0.855	0.732	0.84
$\partial C_L / \partial (\tau\dot{\theta})$	1.41	.30	0.21
$\partial C_M / \partial \alpha$	0.77	0.660	0.85
$\partial C_M / \partial (\tau\dot{\theta})$	- 2.31	- 2.19	0.95

TABLE II

VISCOUS CORRECTIONS FOR STRUCTURAL LOADS

Shear			Bending Moment		
Slender-Body Term		Correction	Slender Body Term		Correction
$\varphi_{S_{z_0}}$		.85	$\varphi_{BM_{G_0}}$		.85
I_{10}	–	.85	I_1	–	.85
I_{11}	–	.80	I_2	–	.75
I_1	–	.78	I_3	–	.85
I_9	–	.85	I_4	–	.85
α_o	–	.85	γ_o	–	.85
β_o	–	.85	δ_o	–	.85

TABLE III

AERODYNAMIC AND PHYSICAL DATA
OF EXAMPLE AIRSHIP

$\partial C_z / \partial \alpha$	= 0.732	M_a	= 2040 slugs
$\partial C_z / \partial (i_T + \alpha)$	= 1.30	I_a	= 8.57×10^6 slug-ft^2
$\partial C_m / \partial \alpha$	= 0.660	k_2	= 0.9
$\partial C_m / \partial (i_T + \alpha)$	= -2.19	k_3	= 1.15
VOL	= 975,000 ft^3	ρ	= 0.002049 slugs/ft^3
L_a	= 339 ft	X_{cg}	= 150 ft
R_M	= 37.7 ft		

TABLE IV

AERODYNAMIC AND PHYSICAL CHARACTERISTICS
OF FOUR NON-RIGID AIRSHIPS

	ZSG-4	ZSG-1	ZPG-2W	ZPG-3W
μ/ρ	1690	1590	1620	1750
λ/ρ	234	250	257	255
r_1	2.16	1.67	1.76	1.76
r_2	-2.88	-2.71	-3.32	-2.63
n	0.307	0.307	0.292	0.291
m	0.00199	0.00186	0.00177	0.00184
$dC_L/d\alpha$	0.670	0.744	0.732	0.678
$dC_L/d(\alpha+\alpha_0)$	1.45	1.24	1.30	1.193
$dC_m/d\alpha$	0.759	0.717	0.640	0.735
$dC_m/d(\alpha+\alpha_0)$	-2.17	-1.94	-2.19	-2.078
vol - ft^3	527,000	650,000	975,000	1,445,000
L_s - ft	263	282	339	403.4
R_M - ft	31.1	33.8	37.7	42.6
I_a (additional) slug-ft^2	4,410,000	6,300,000	12,350,000	29,000,000
I_o (physical) slug-ft^2	3,760,000	5,370,000	10,520,000	21,000,000
k_1	0.870	0.869	0.869	0.885
k_3	1.17	1.17	1.17	1.38
M_a (additional)-lugs	1215	1600	2972	3440
M_o (physical) slugs	1250	1550	2300	3500
M total slugs	2465	3150	4572	6940

TABLE V

PHYSICAL AND APPARENT MASS INTEGRALS FOR
SHEAR AND BENDING MOMENT EXPRESSIONS

Shear

Station	I_{10}	I_{11}	I_1	I_7/f	I_9	I_8/f
0.2065	3562	- 471	422	238	137.0	89.5
0.3540	4422	570	1026	630	242.0	136.3
0.4572	4403	1485	1485	1703	266.0	181.1
0.5900	3819	2544	2037	2414	230.0	164.3
0.7080	2925	3171	2437	2571	154.0	121.9
0.8171	1900	3385	2702	2689	74.46	108.3

Bending Moment

Station	I_2	I_3	I_6/f	I_4	I_5/f
0.2065	-105.8	11.08	9.31	30.96	22.86
0.3540	-105.8	39.86	25.38	136.2	94.61
0.4572	0.0	66.31	43.33	263.6	193.11
0.5900	270.5	100.2	66.00	500.2	495.9
0.7080	611.2	123.1	84.50	772.2	790.4
0.8171	972.3	135.2	97.80	1046.0	1069.0

$\rho = 0.002049$ slugs/ft^3

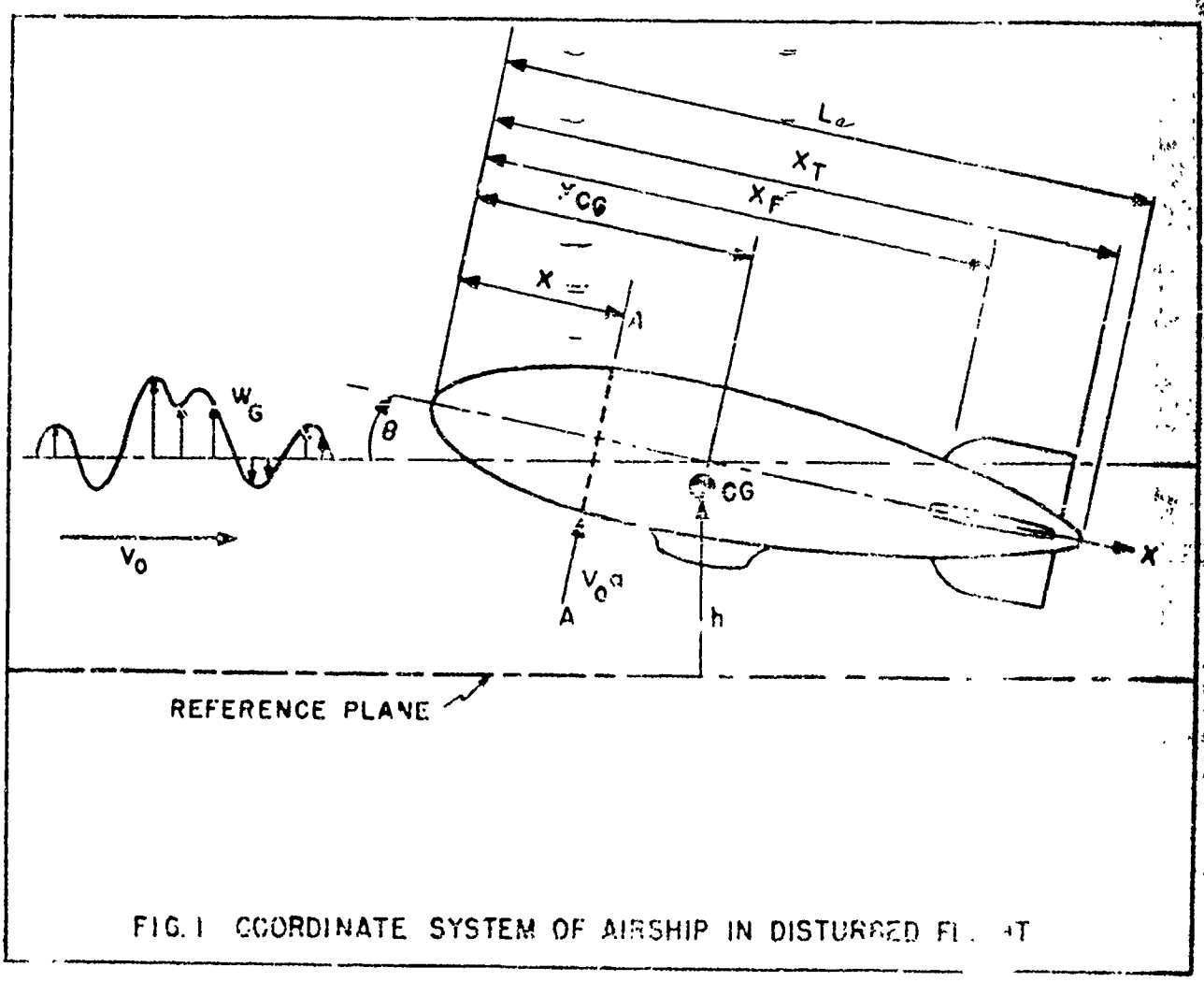

FIG. 1 COORDINATE SYSTEM OF AIRSHIP IN DISTURBED FLIGHT

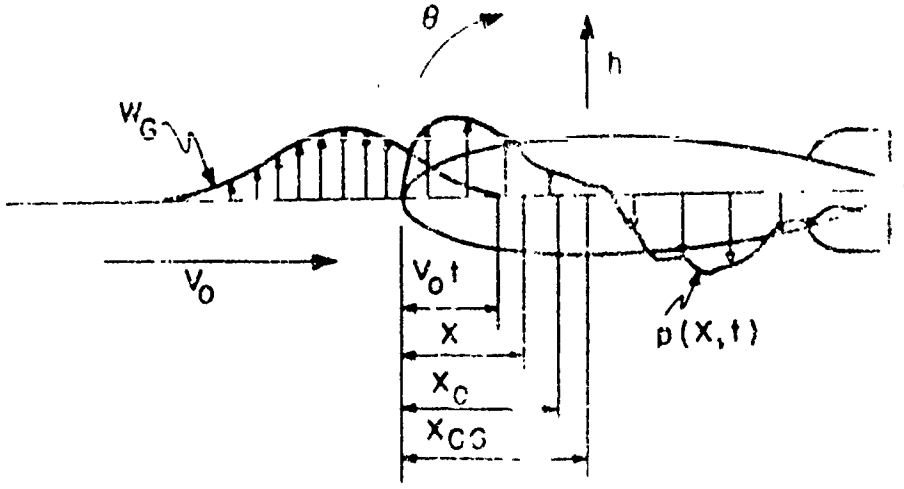

FIG. 2 LOADING DIAGRAM OF AIRSHIP

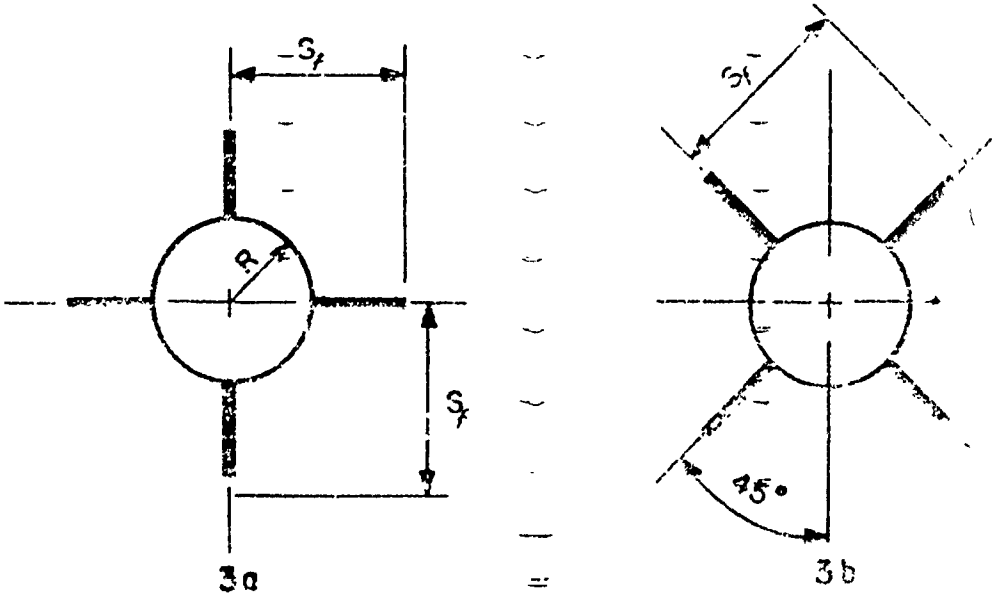

FIG. 3 TAIL-FIN CONFIGURATIONS

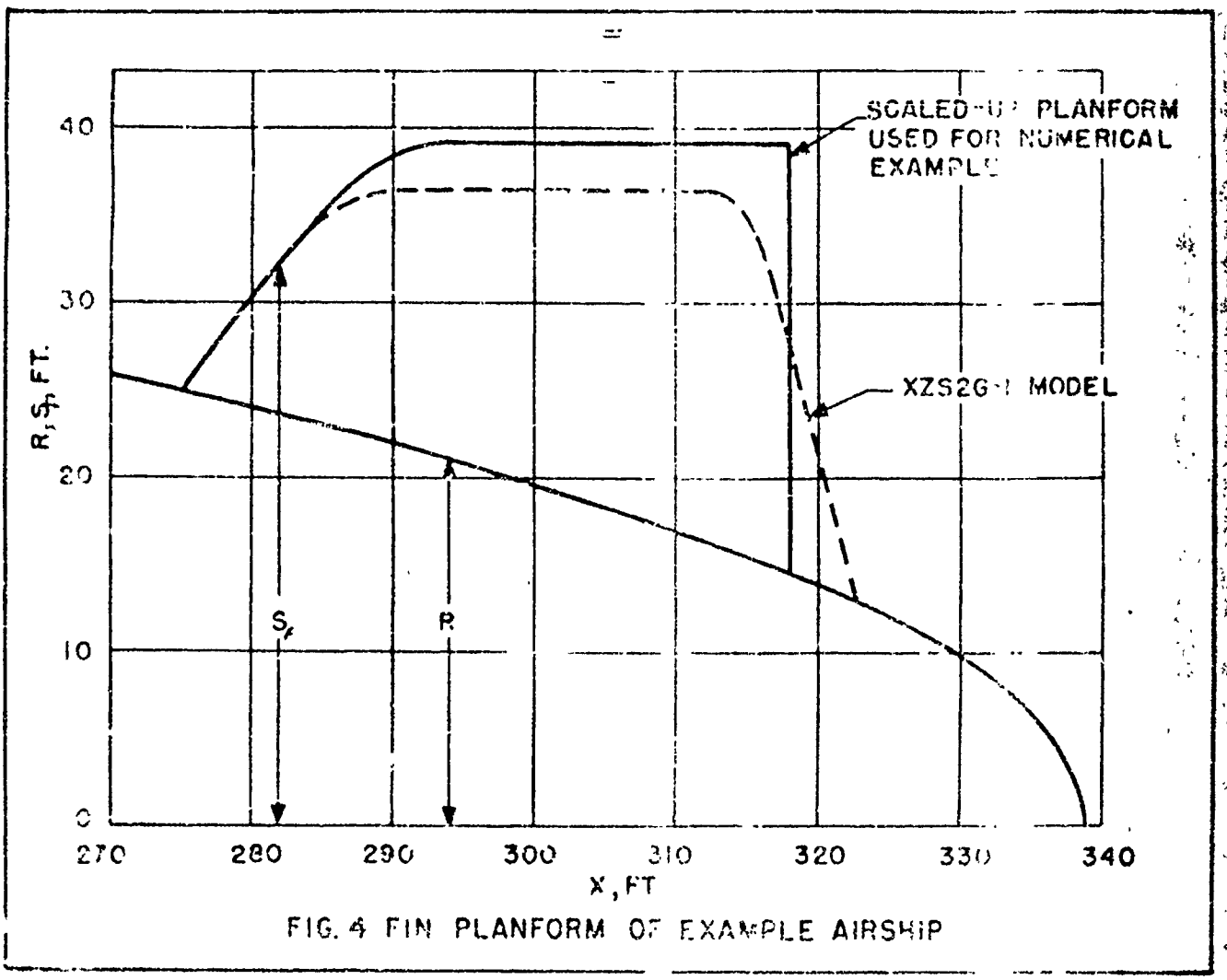

FIG. 4 FIN PLANFORM OF EXAMPLE AIRSHIP

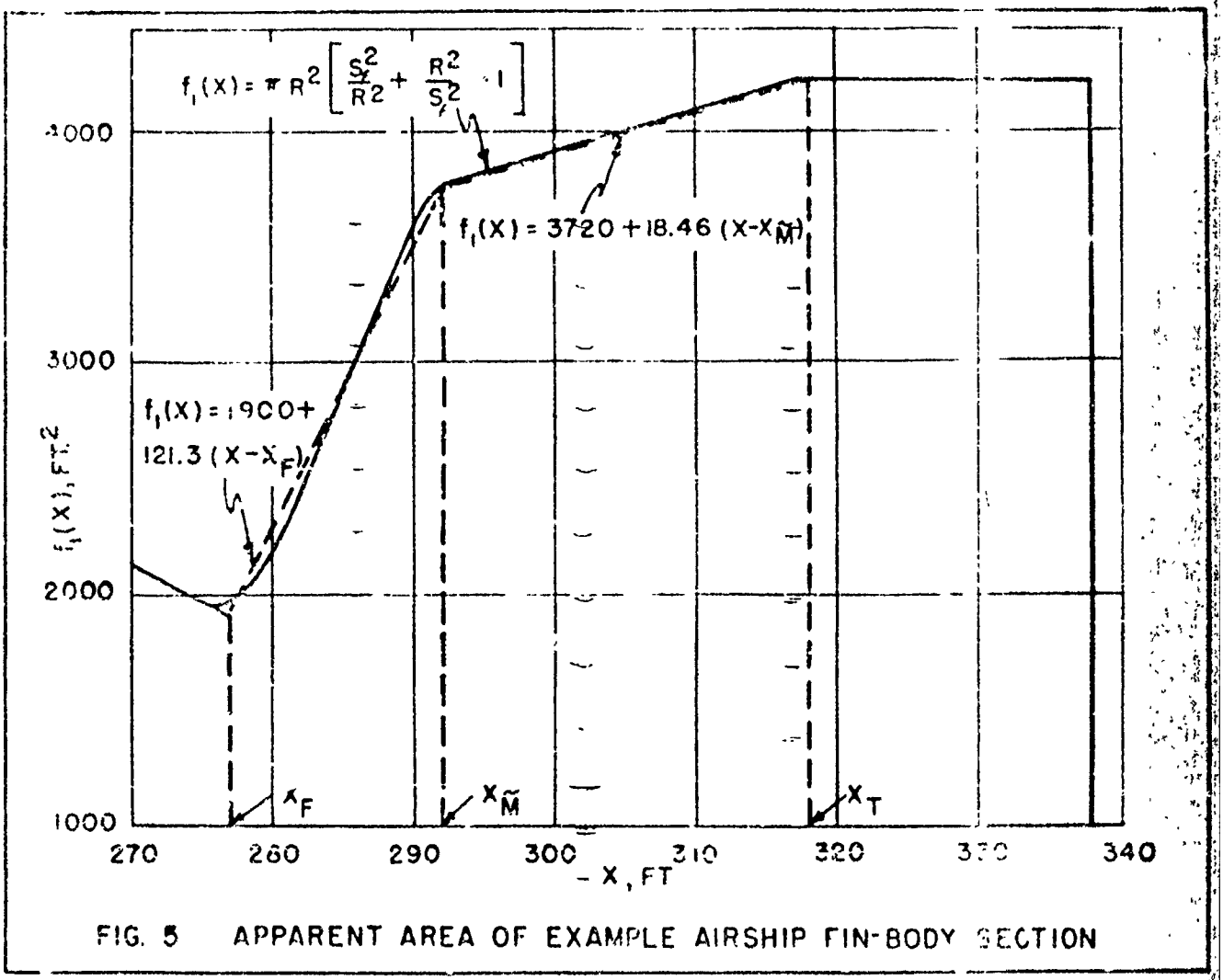

FIG. 5 APPARENT AREA OF EXAMPLE AIRSHIP FIN-BODY SECTION

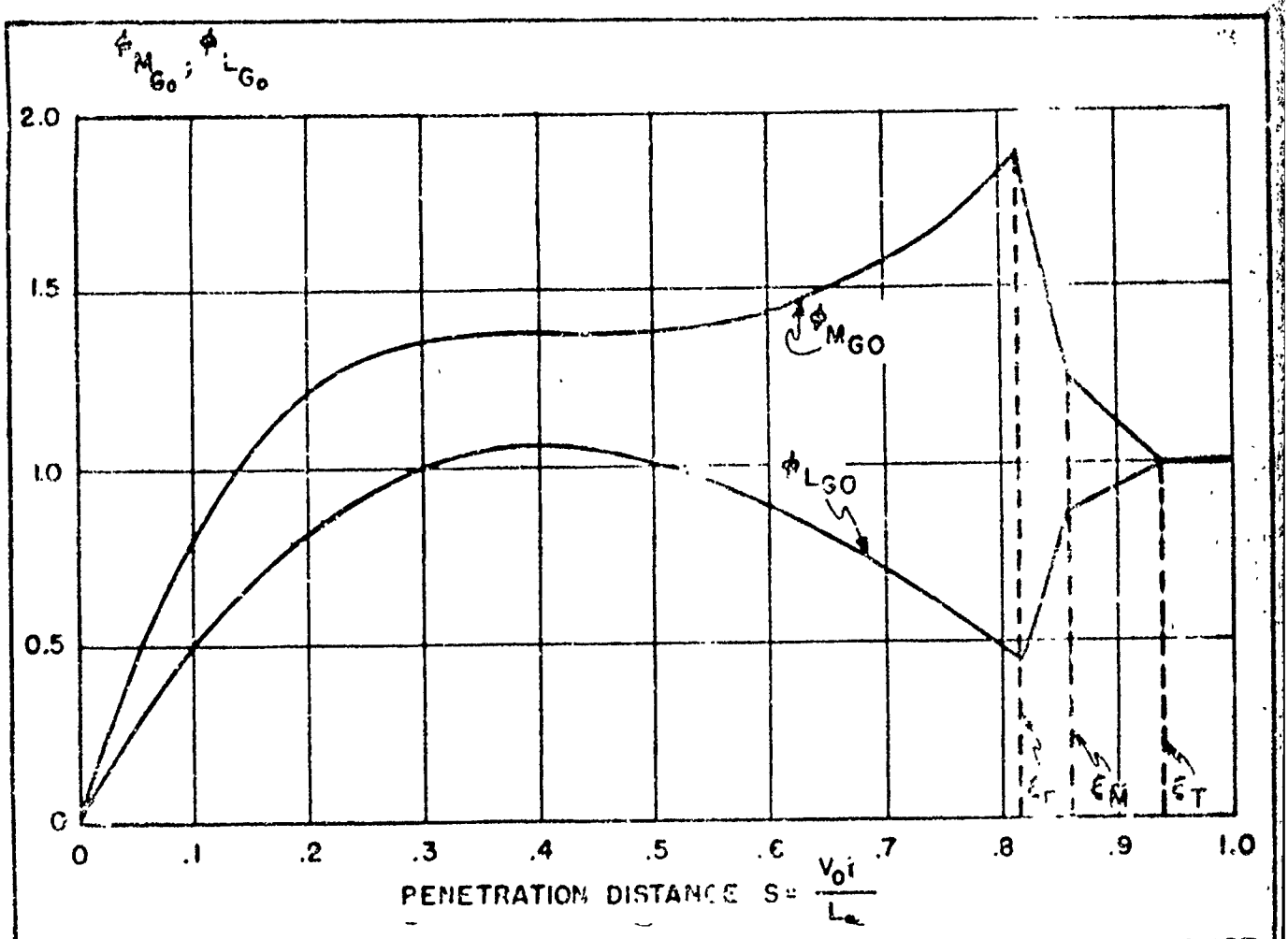

FIG. 6 LIFT AND PITCHING MOMENT DUE TC PENETRATION OF SHARP-EDGED GUST

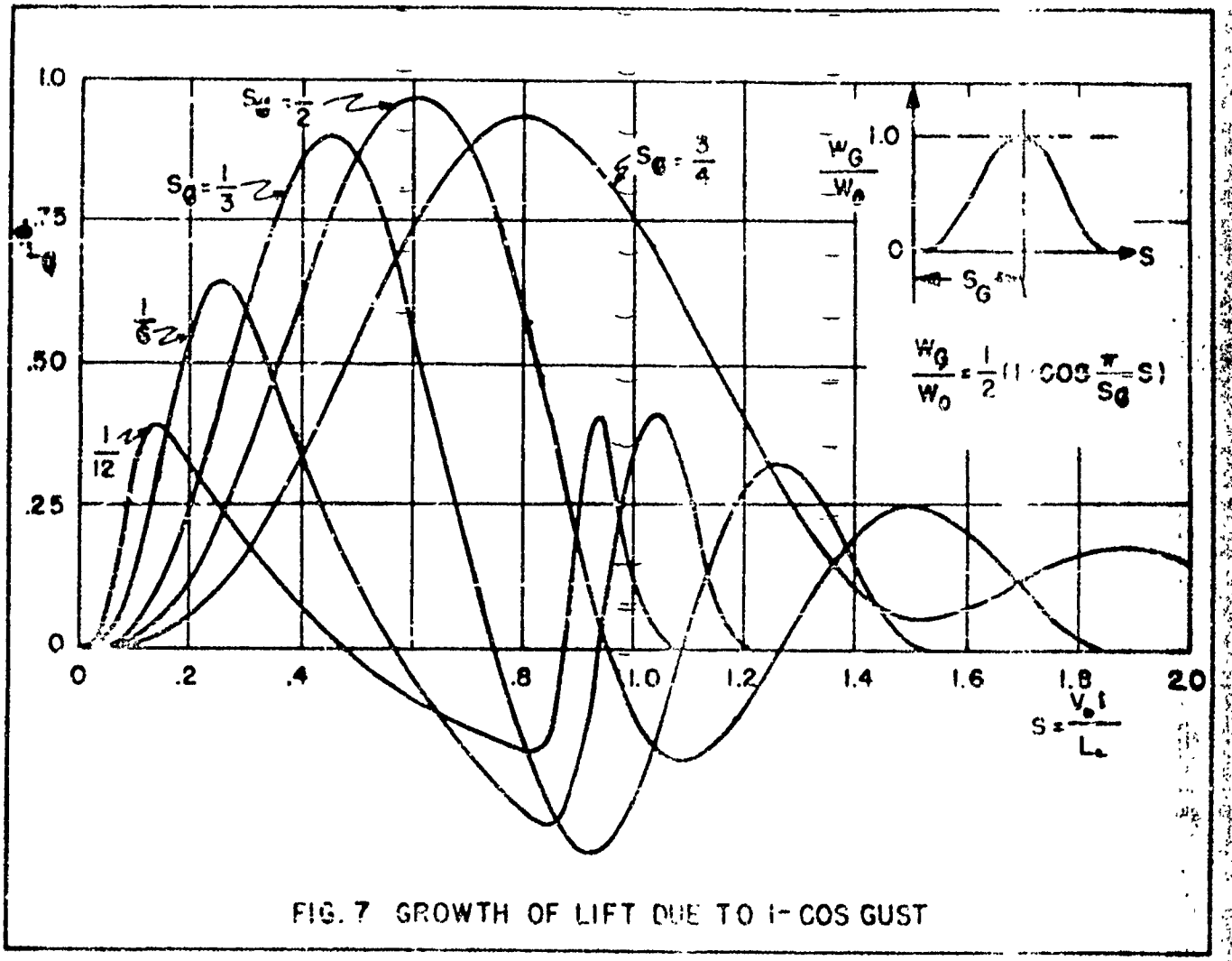

FIG. 7 GROWTH OF LIFT DUE TO 1-COS GUST

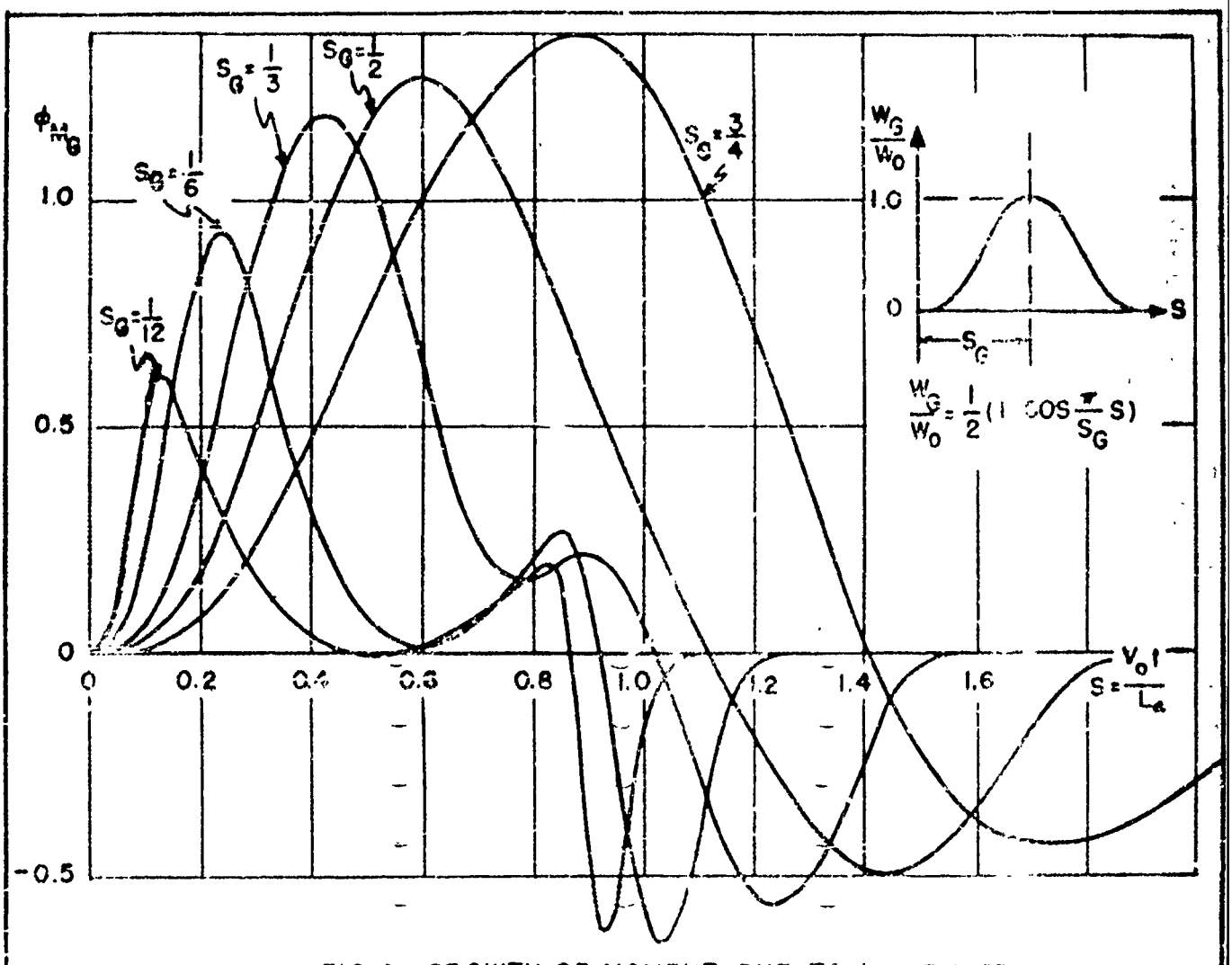

FIG. 8 GROWTH OF MOMENT DUE TO 1-COS GUST

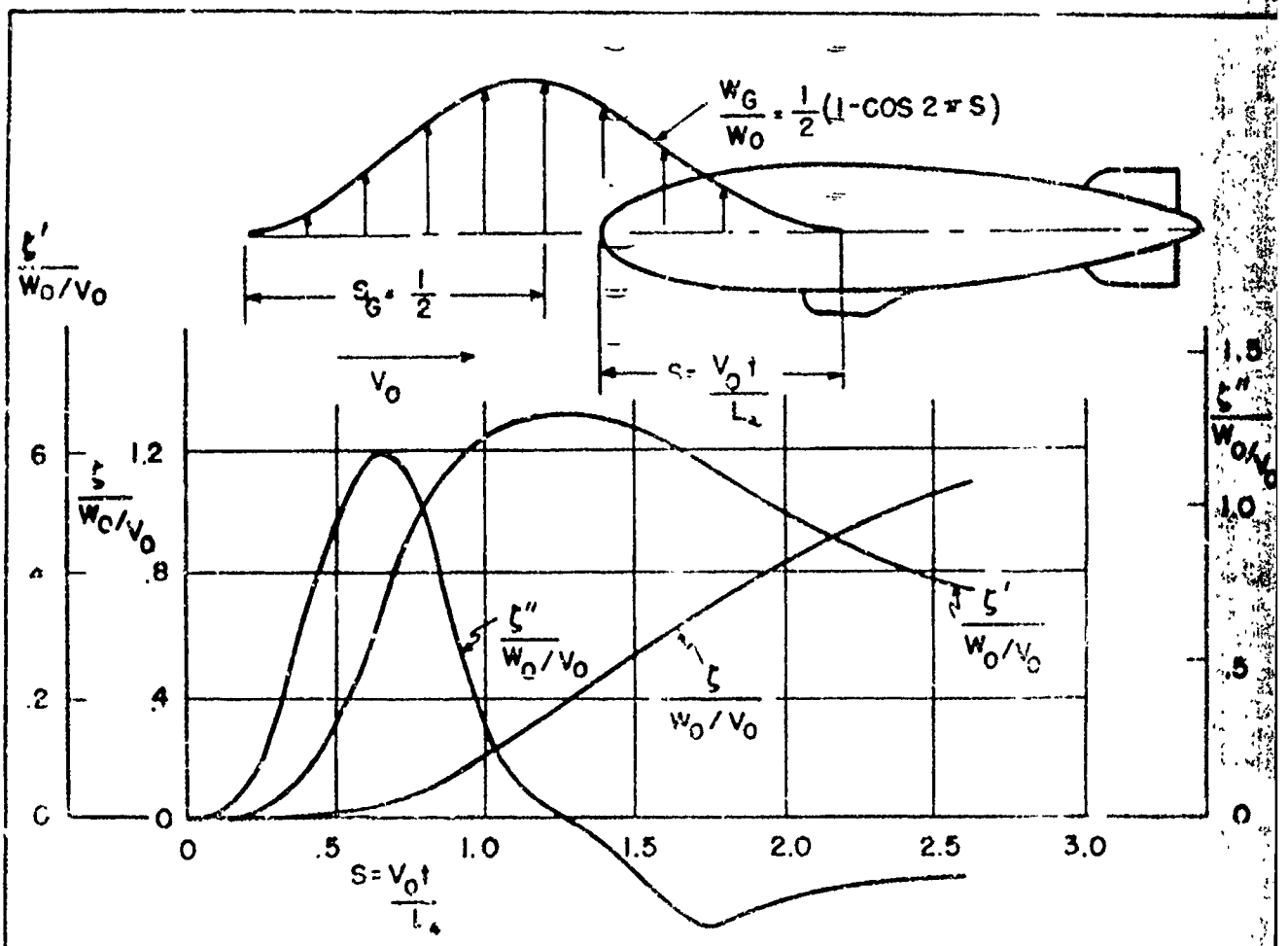

FIG. 9 VERTICAL RESPONSE TO 1-COS GUST, $S_G = \frac{1}{2}$

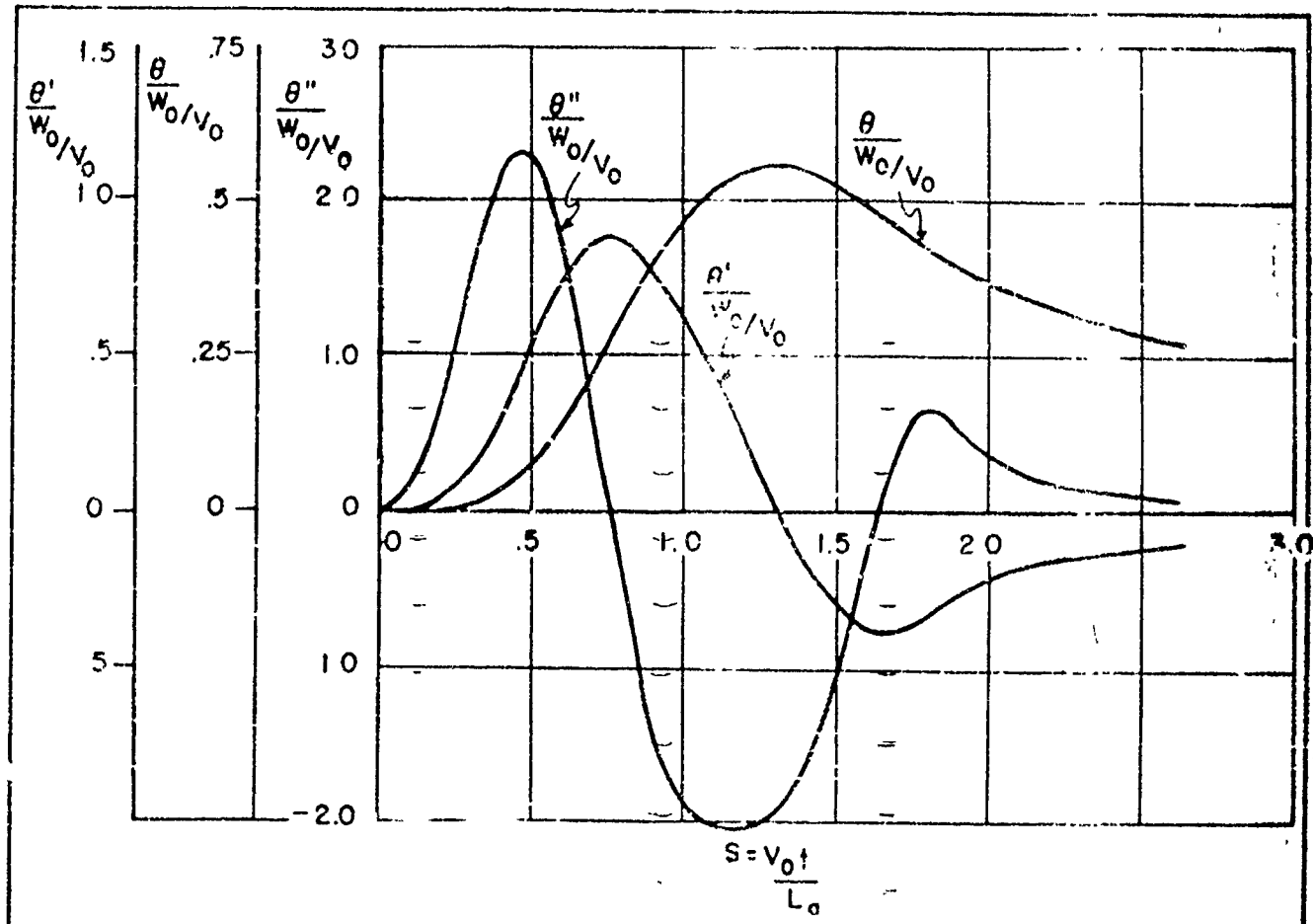

FIG 10 PITCHING RESPONSE TO 1-COS GUST, $\sigma_G = \frac{1}{2}$

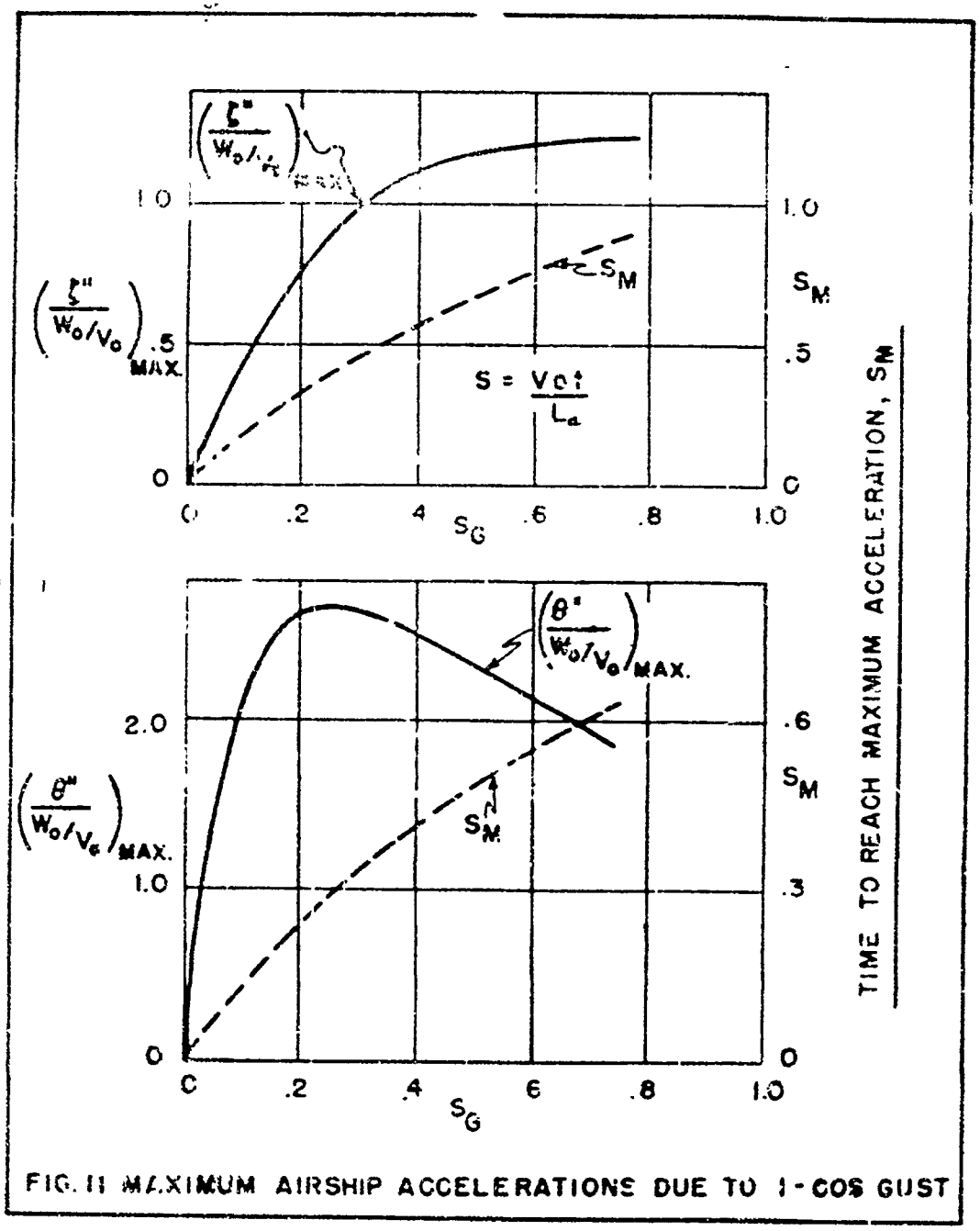

FIG. 11 MAXIMUM AIRSHIP ACCELERATIONS DUE TO 1-COS GUST

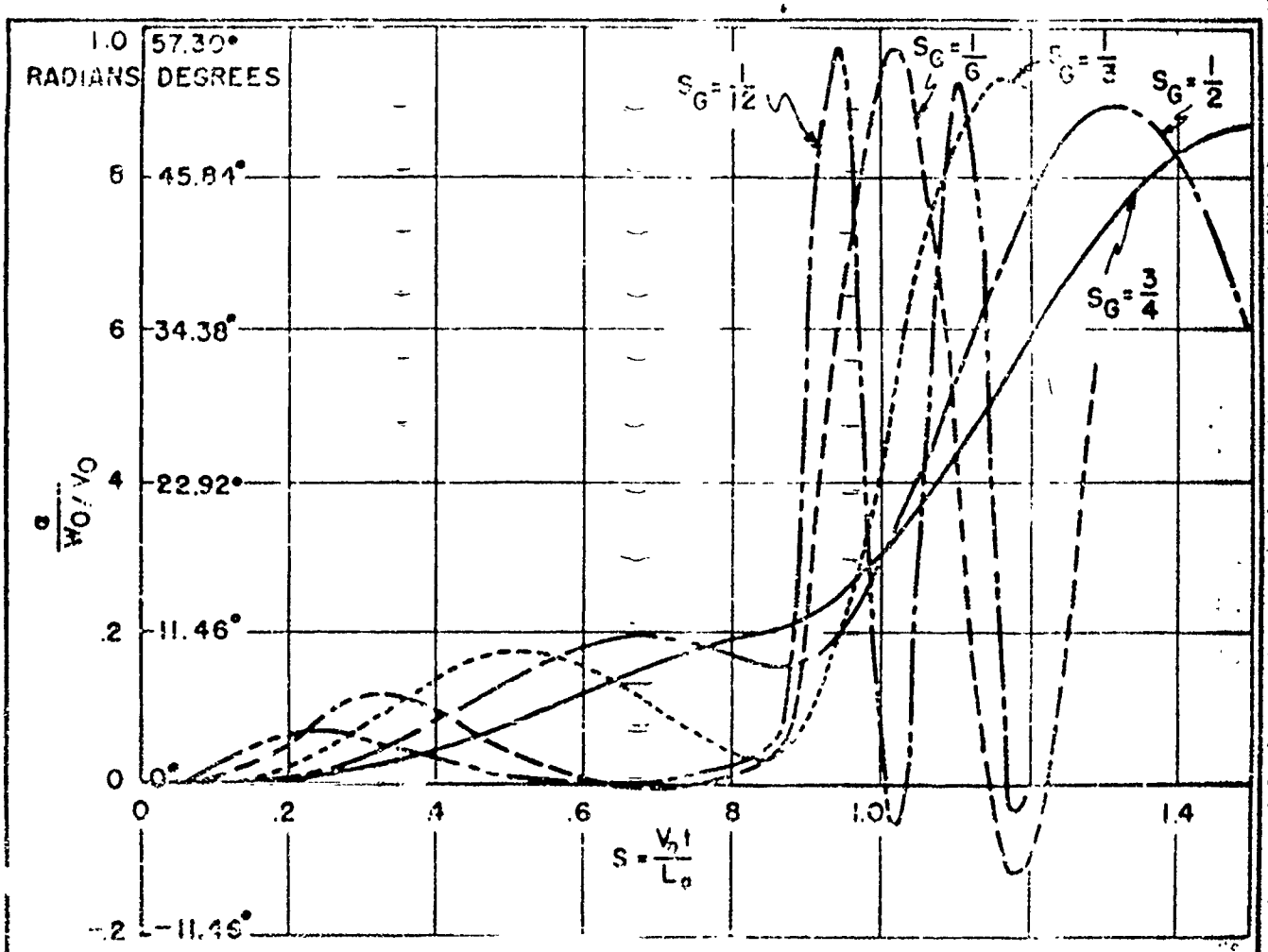

FIG. 12 ANGLE OF ATTACK AT CENTER OF PRESSURE OF FIN DUE TO 1-COS GUST

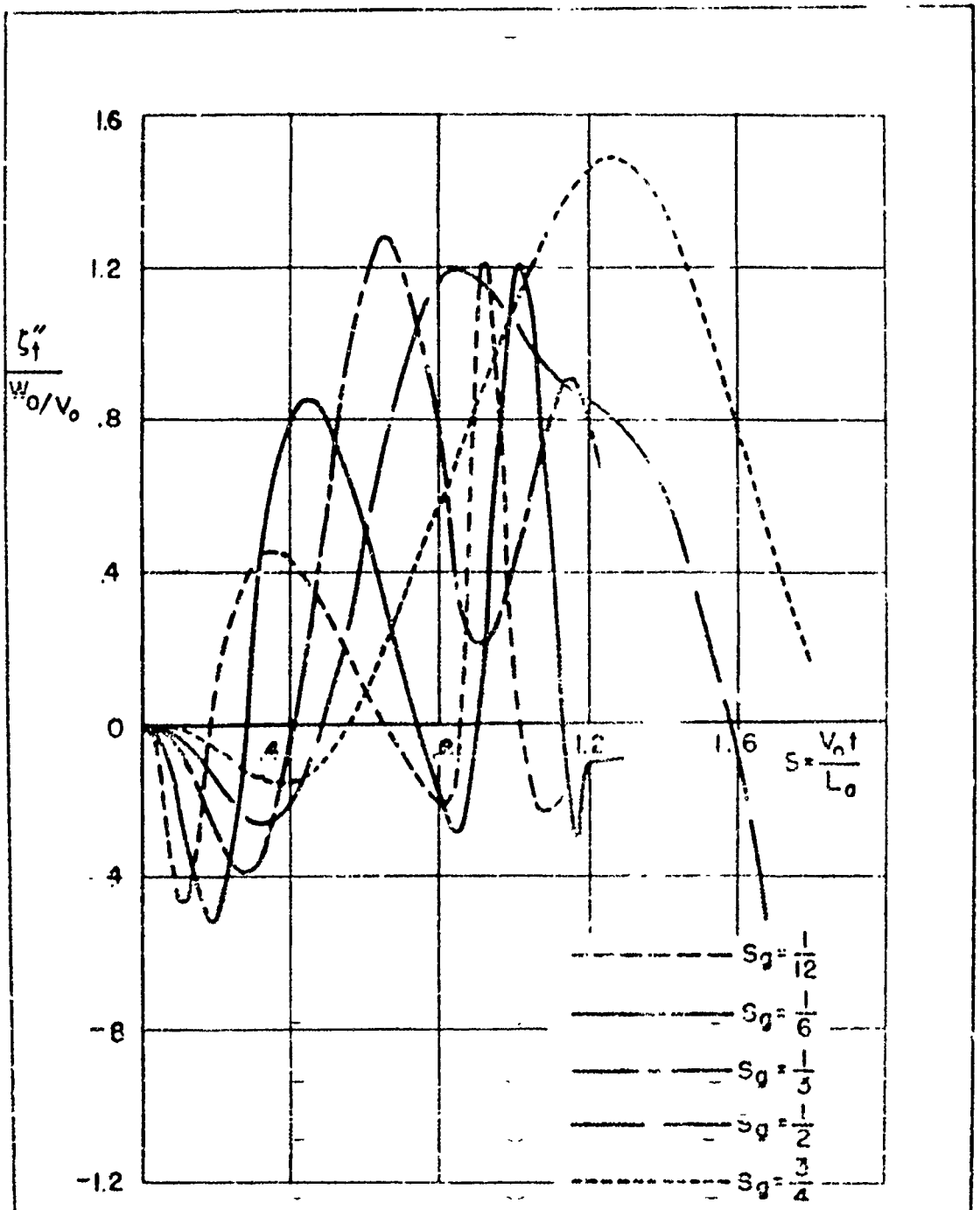

FIG. 13 VERTICAL ACCELERATION AT CENTER OF PRESSURE OF FIN DUE TO 1-COS GUST

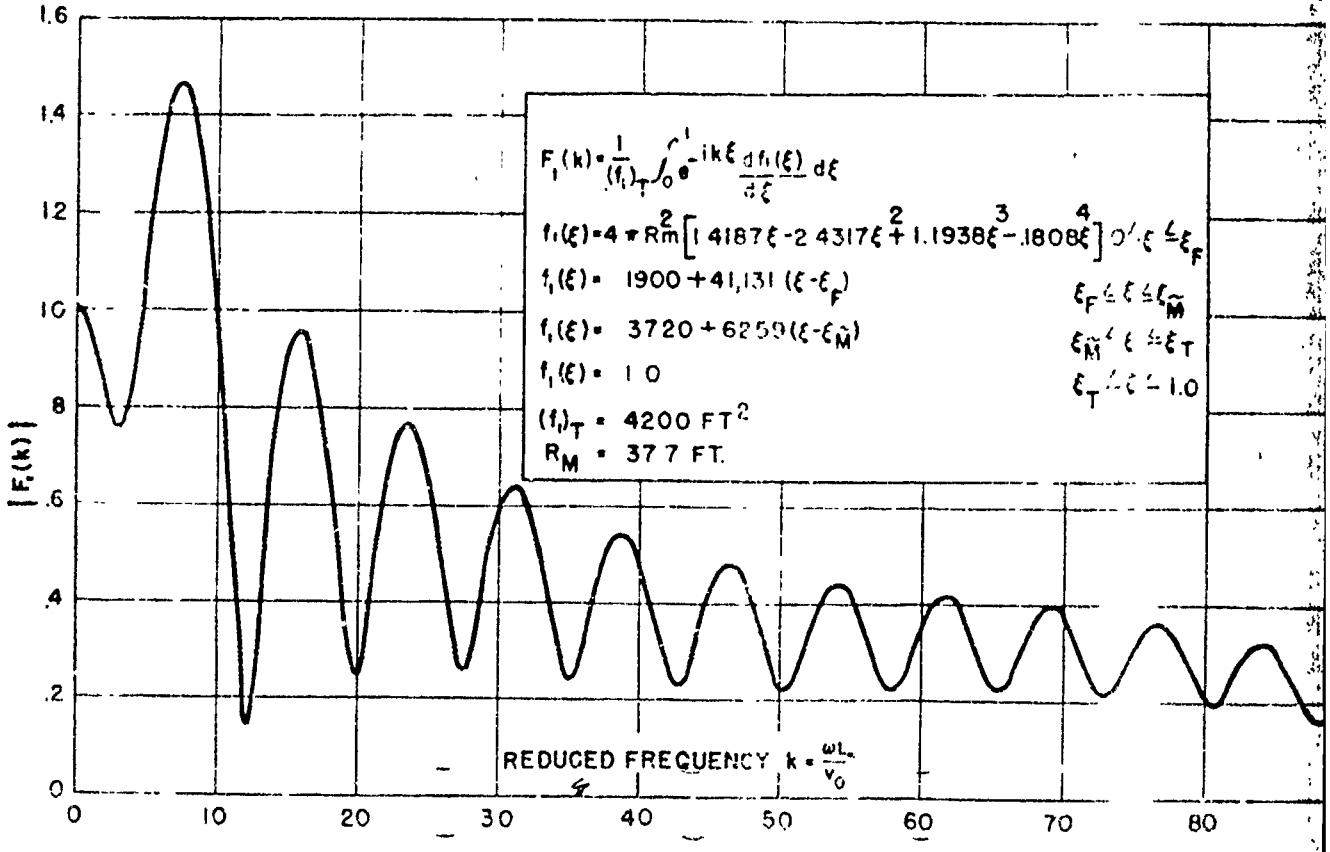

FIG 14 ABSOLUTE VALUE OF STEADY STATE LIFT FUNCTION $F_1(k)$

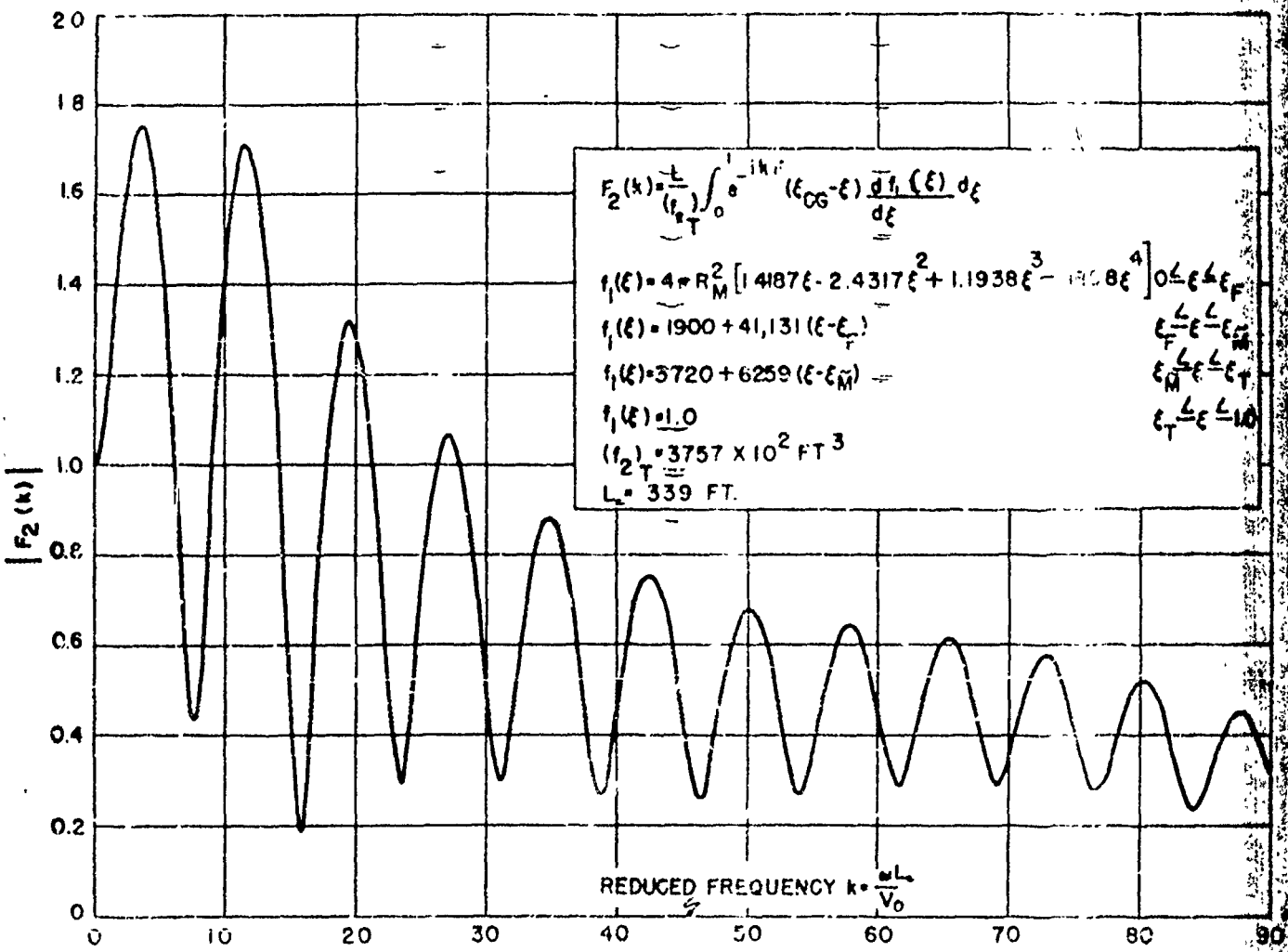

FIG. 15 ABSOLUTE VALUE OF STEADY-STATE PITCHING MOMENT FUNCTION $F_2(k)$

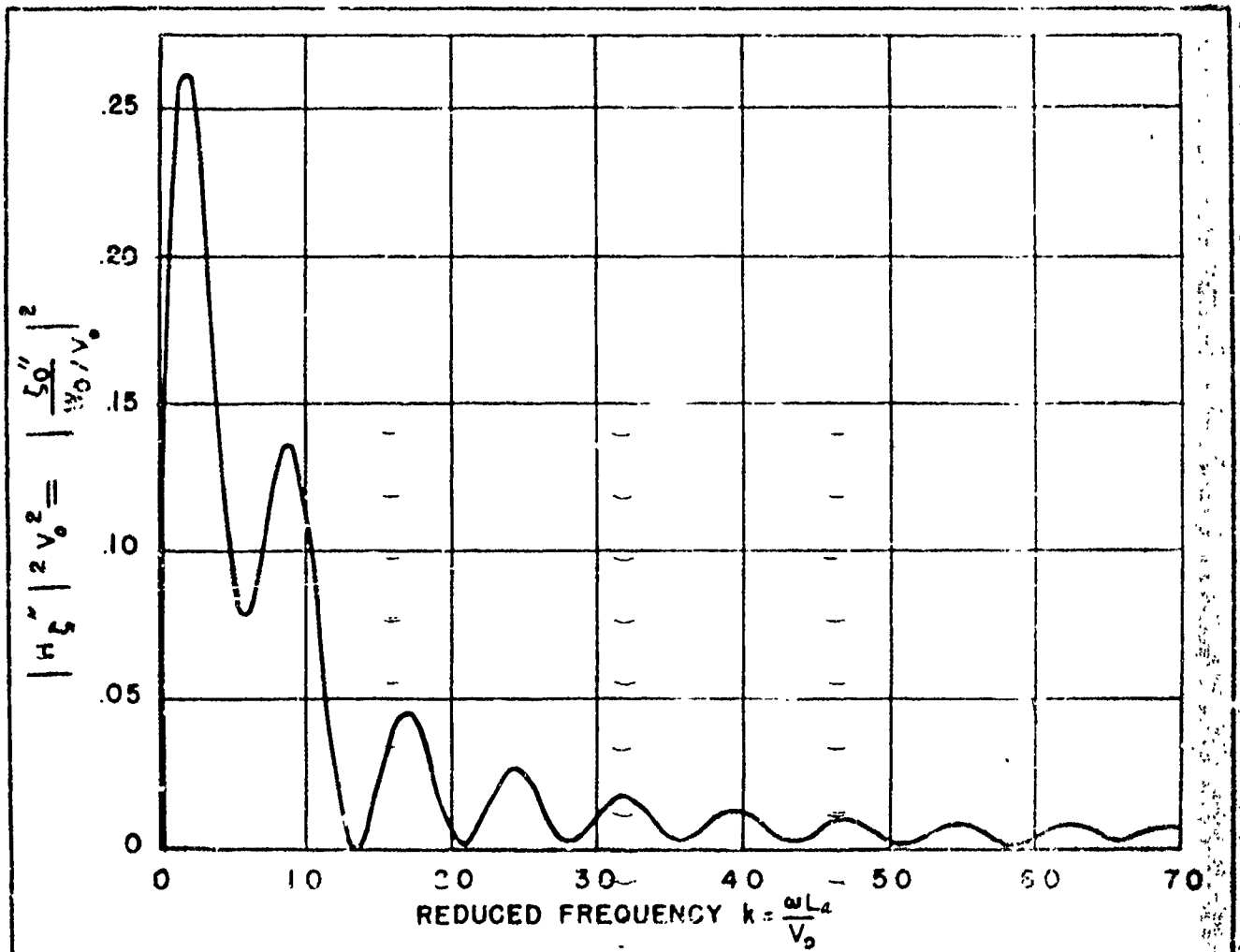

FIG.16 TRANSFER FUNCTION WITH RESPECT TO VERTICAL ACCELERATION

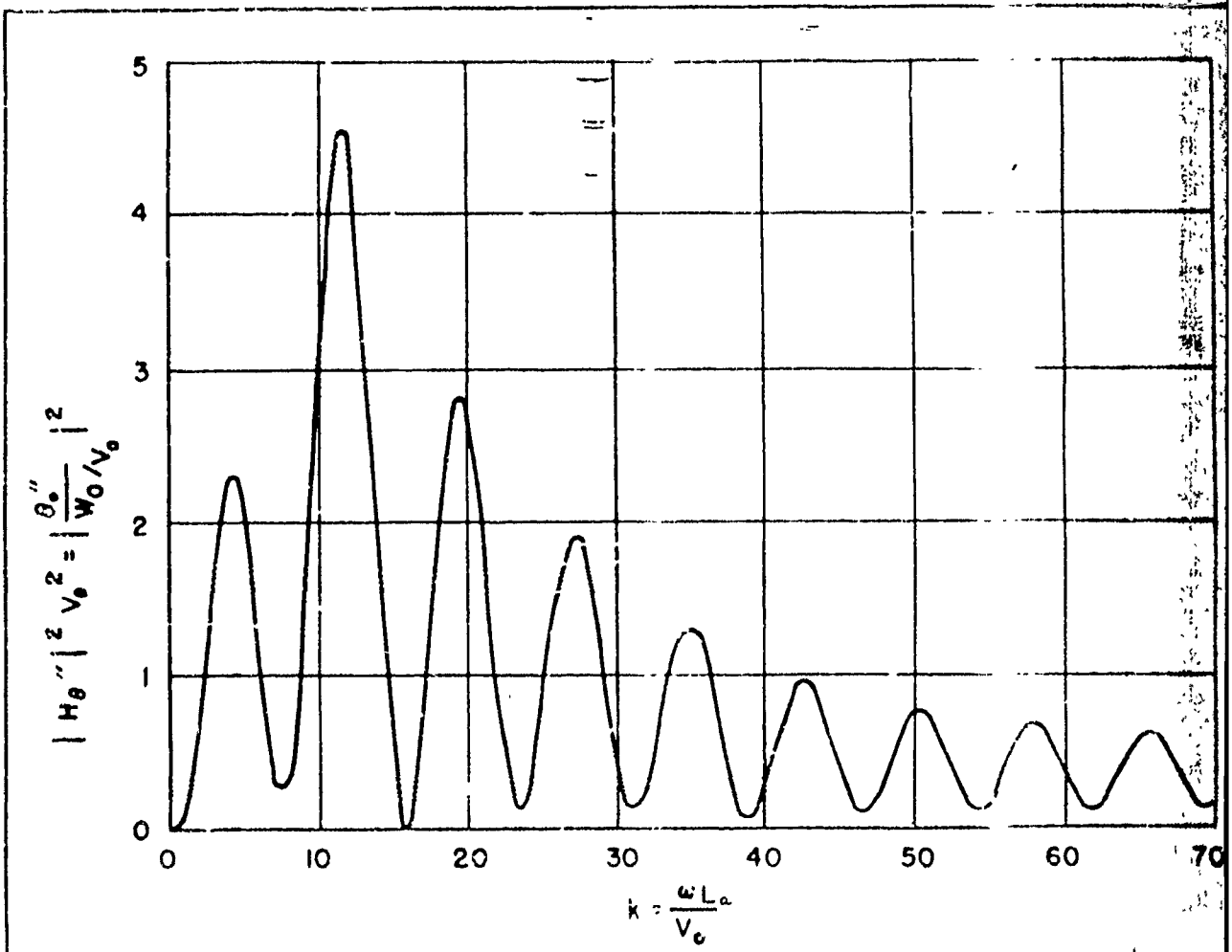

FIG. 17 TRANSFER FUNCTION WITH RESPECT TO PITCH ACCELERATION

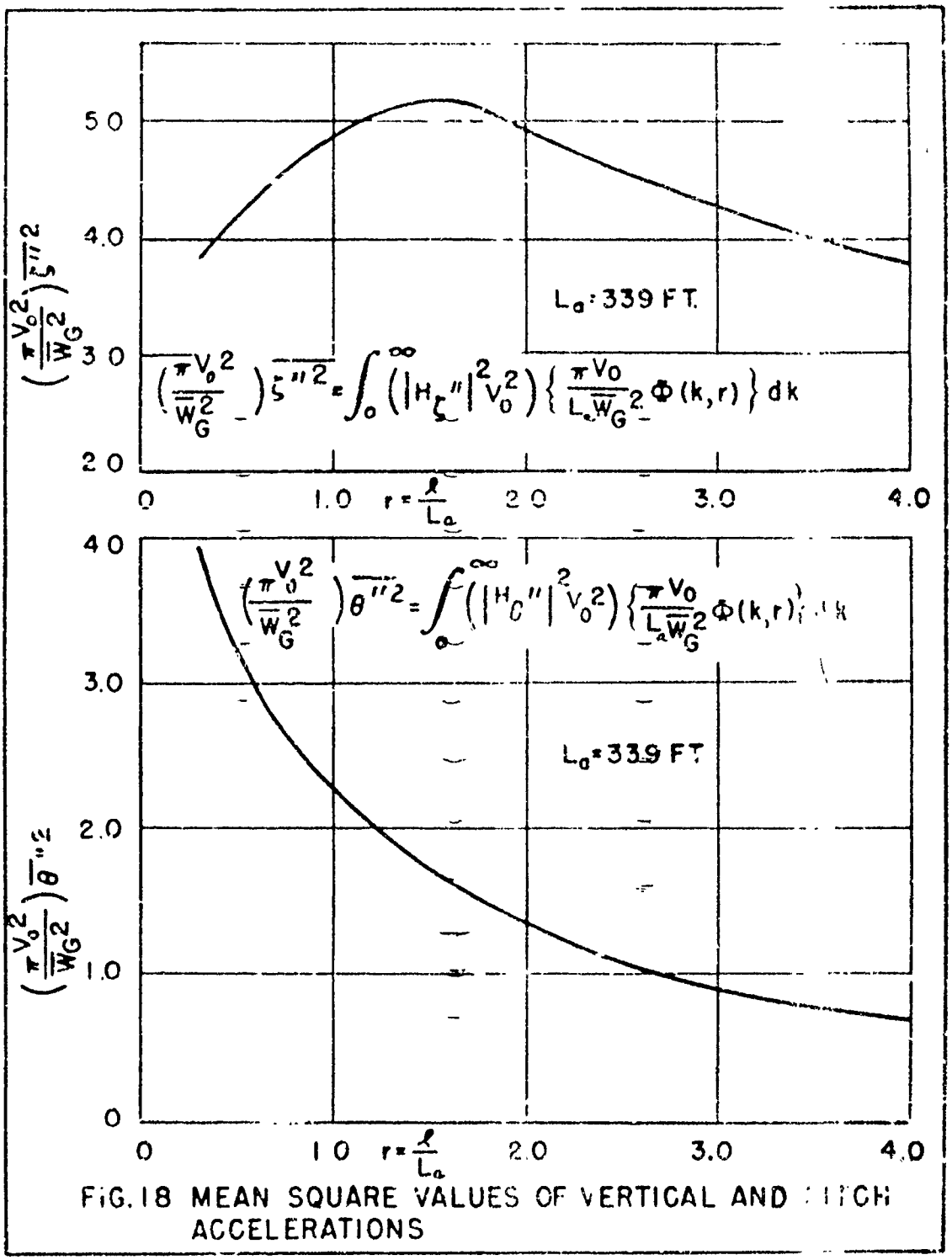

FIG. 18 MEAN SQUARE VALUES OF VERTICAL AND PITCH ACCELERATIONS

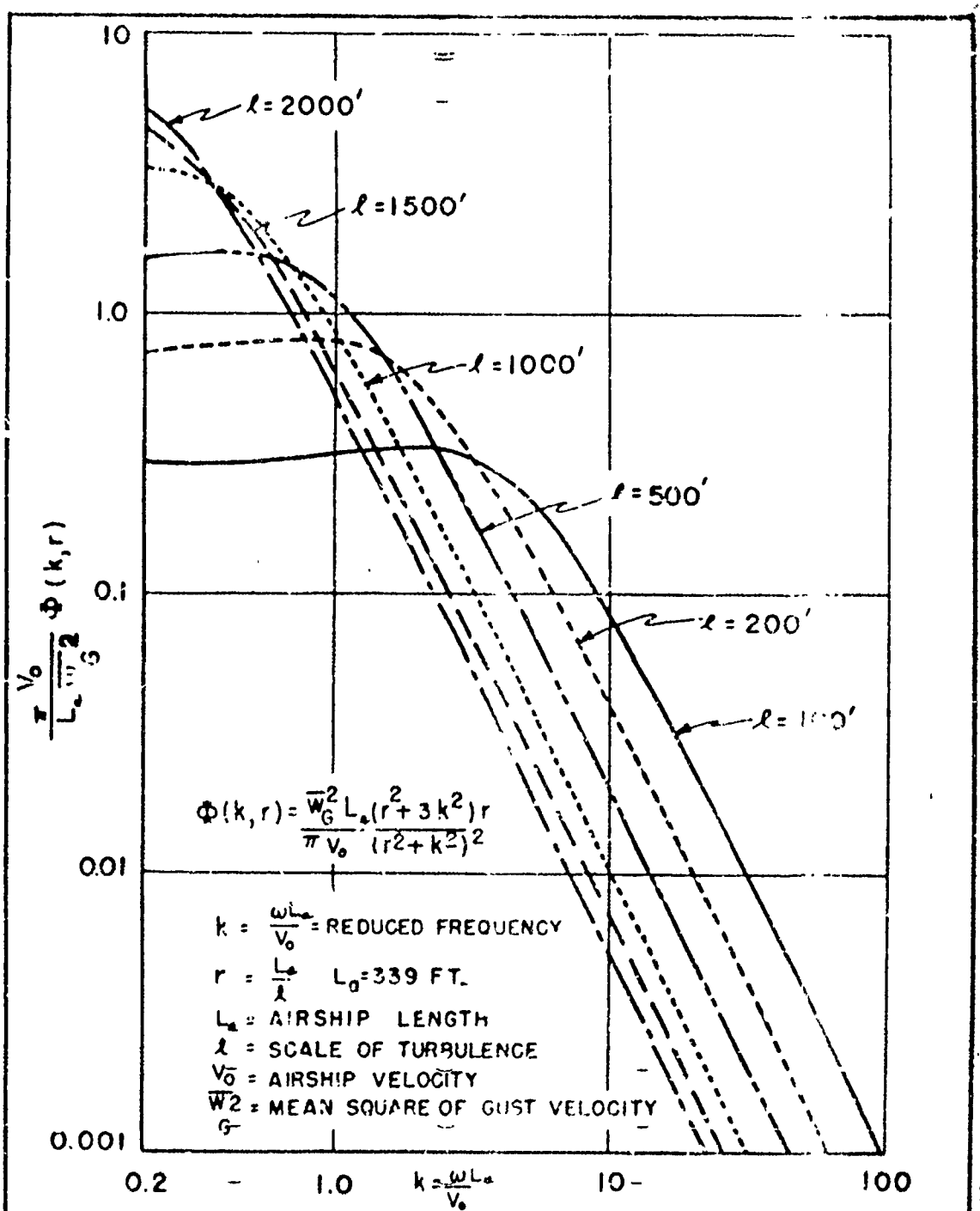

FIG. 19 POWER SPECTRAL DENSITY OF VERTICAL GUST DISTURBANCE

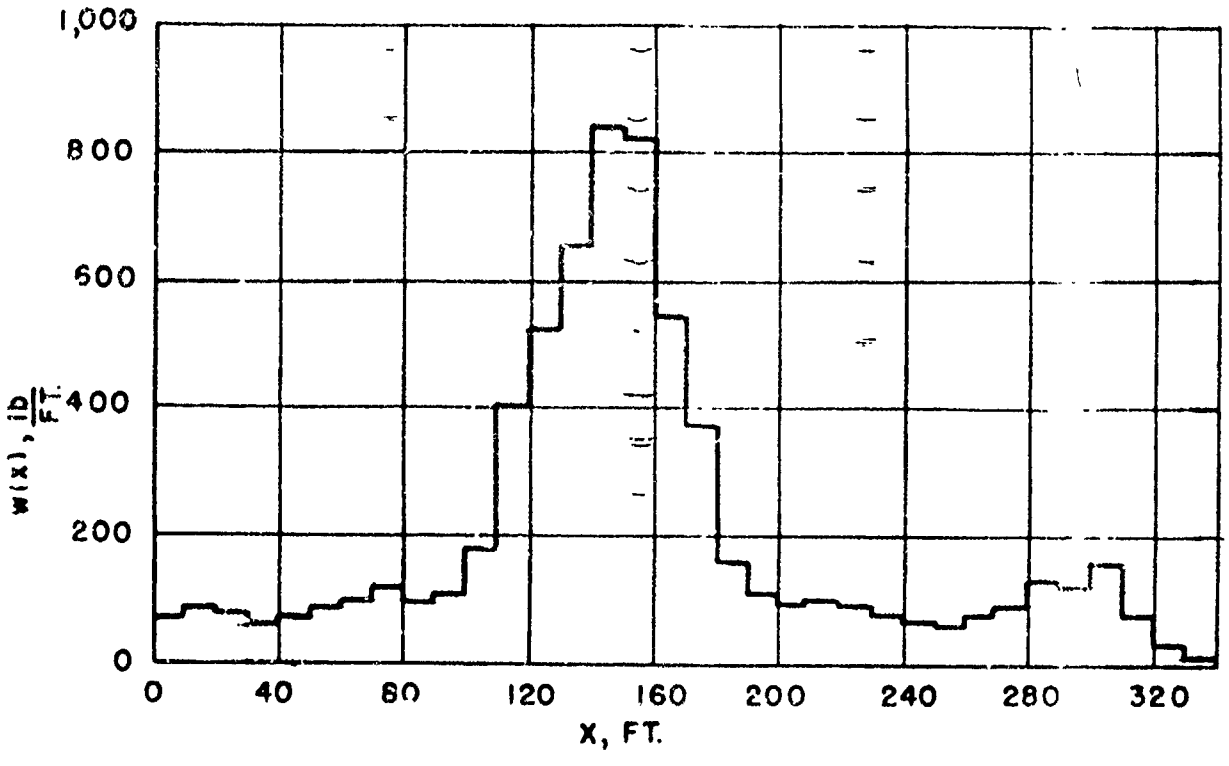

FIG.20 DISTRIBUTED WEIGHT OF EXAMPLE AIRSHIP

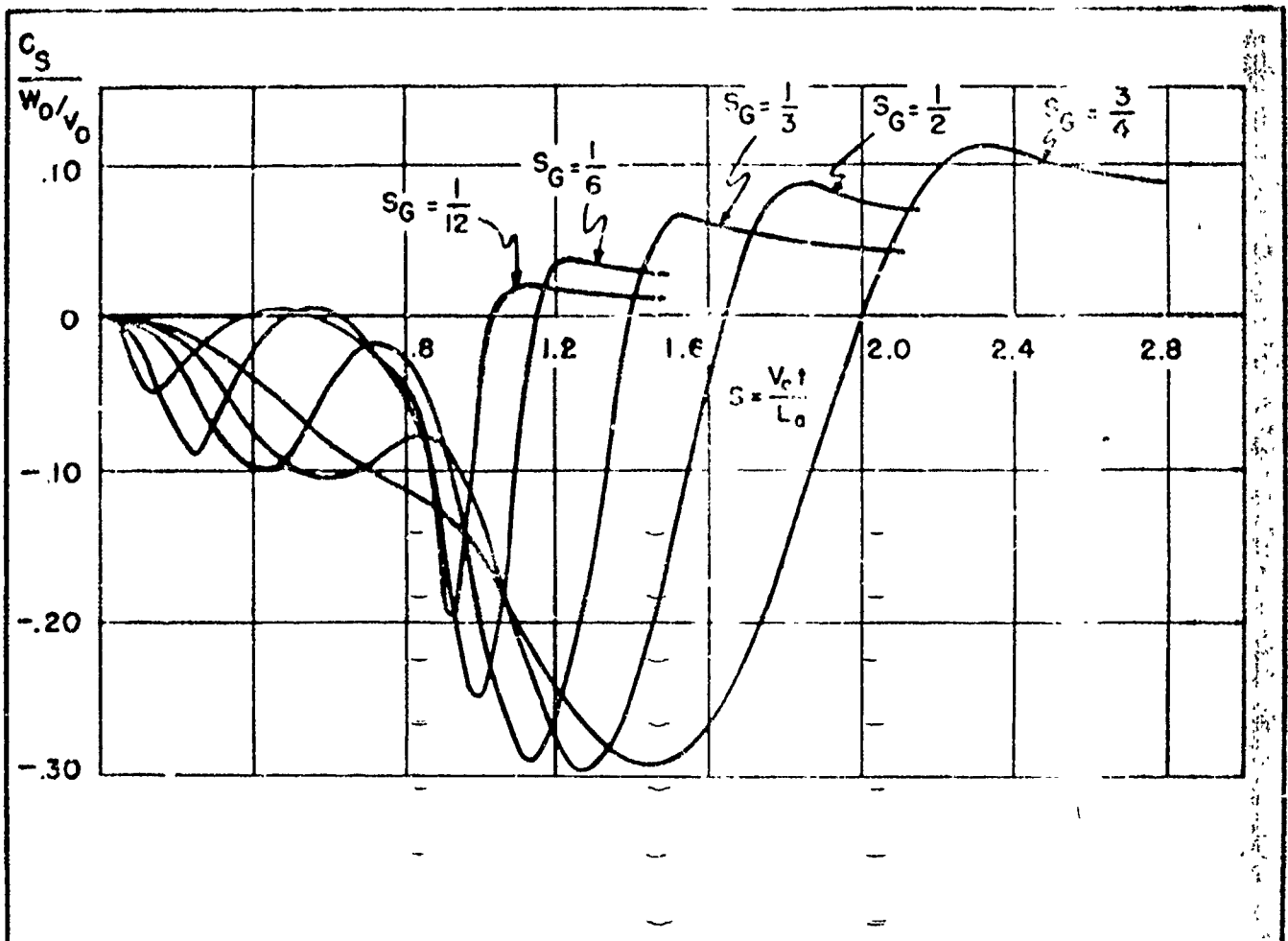

FIG. 21 SHEAR COEFFICIENT AT STATION $\xi_0 = .817L$ DUE TO 1-COS GUST

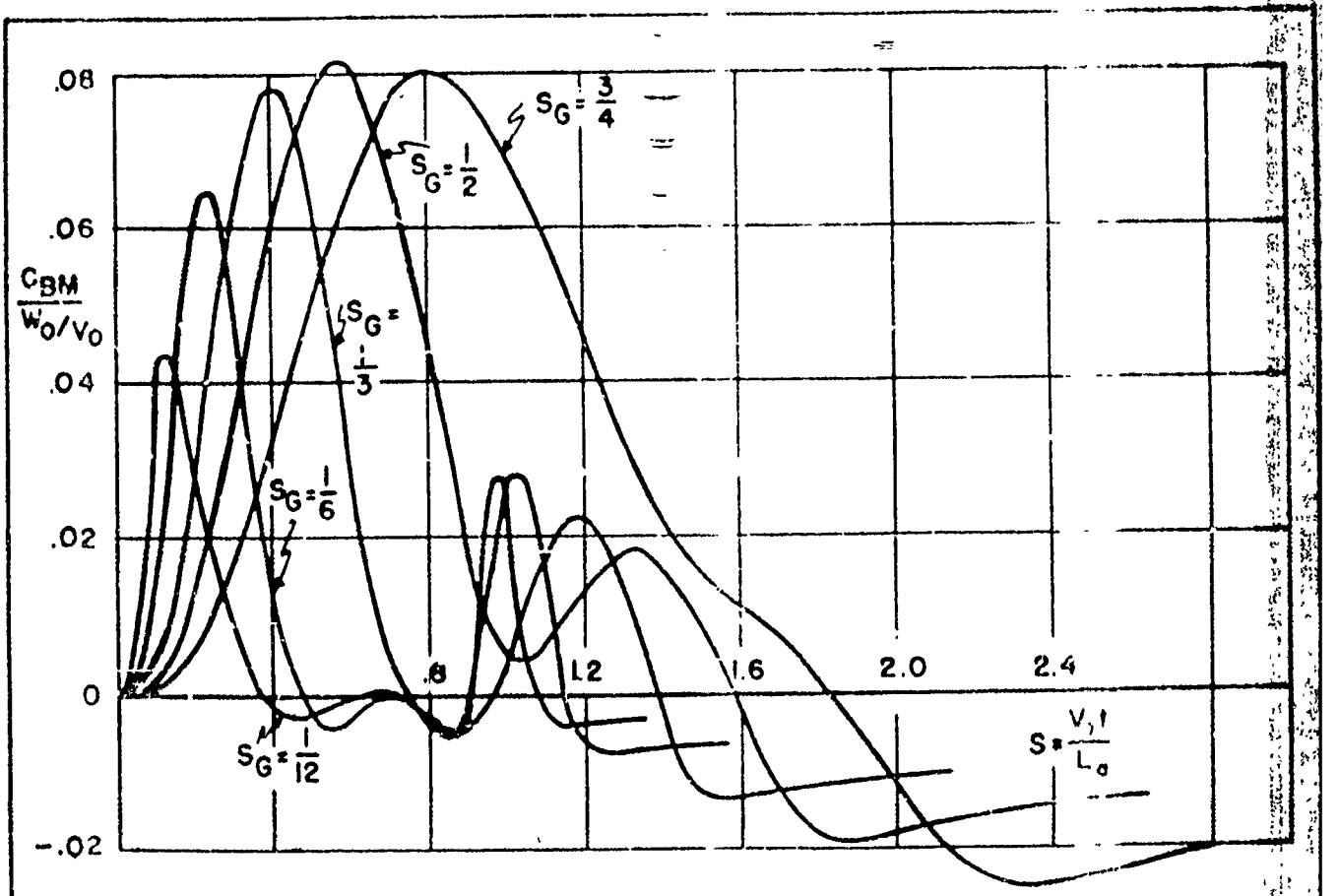

FIG. 22 BENDING MOMENT COEFFICIENT AT STATION $\xi_0 = .4572$ DUE TO 1-COS GUST

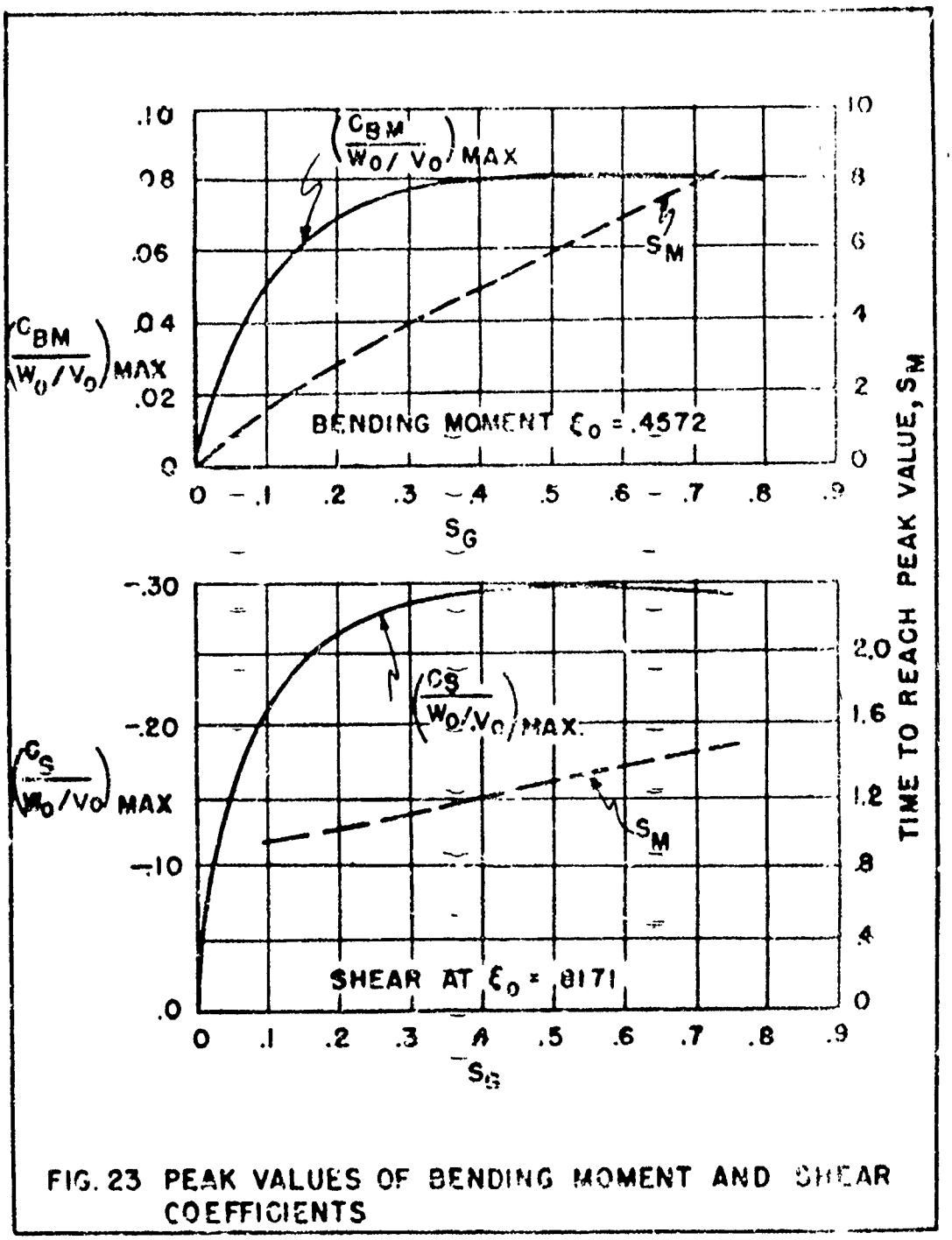

FIG. 23 PEAK VALUES OF BENDING MOMENT AND SHEAR COEFFICIENTS

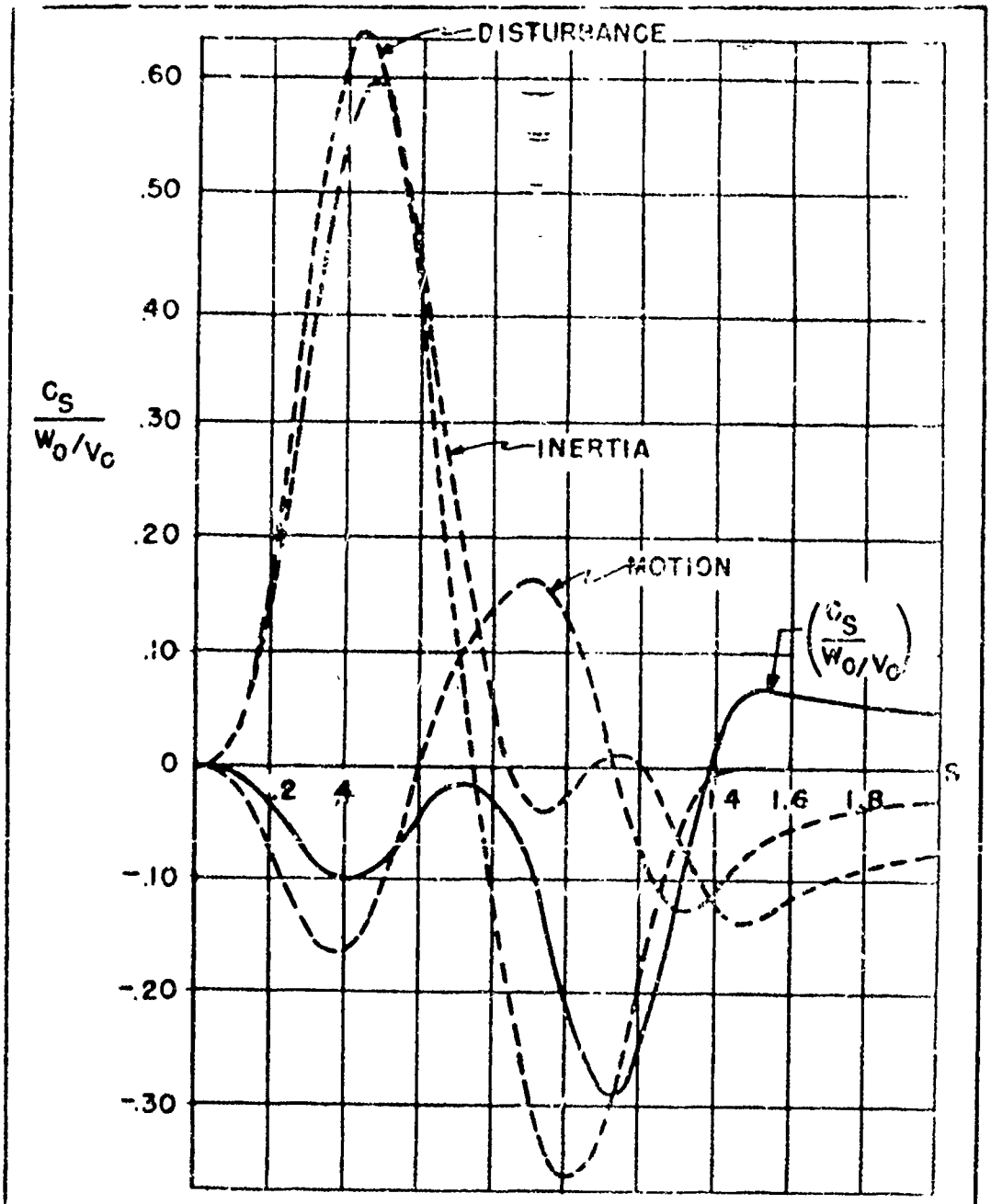

FIG 24 SHEAR COEFFICIENT AT STATION $\zeta_0 = .8171$ DUE TO 1-COS GUST, $S_G =$

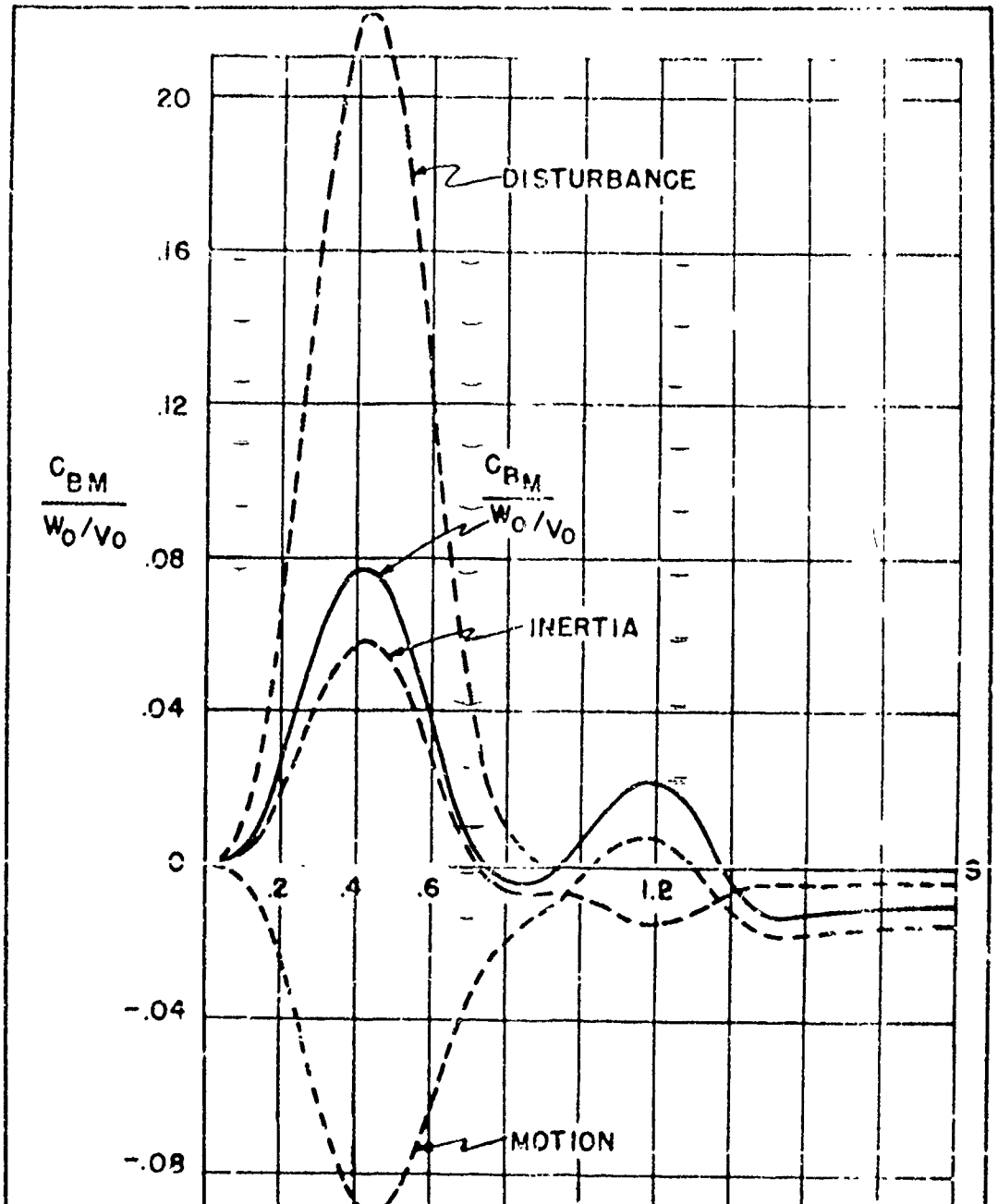

FIG. 25 BENDING MOMENT COEFFICIENT AT STATION ζ_0 .4572 DUE TO 1- COS GUST, $S_G = \frac{1}{3}$

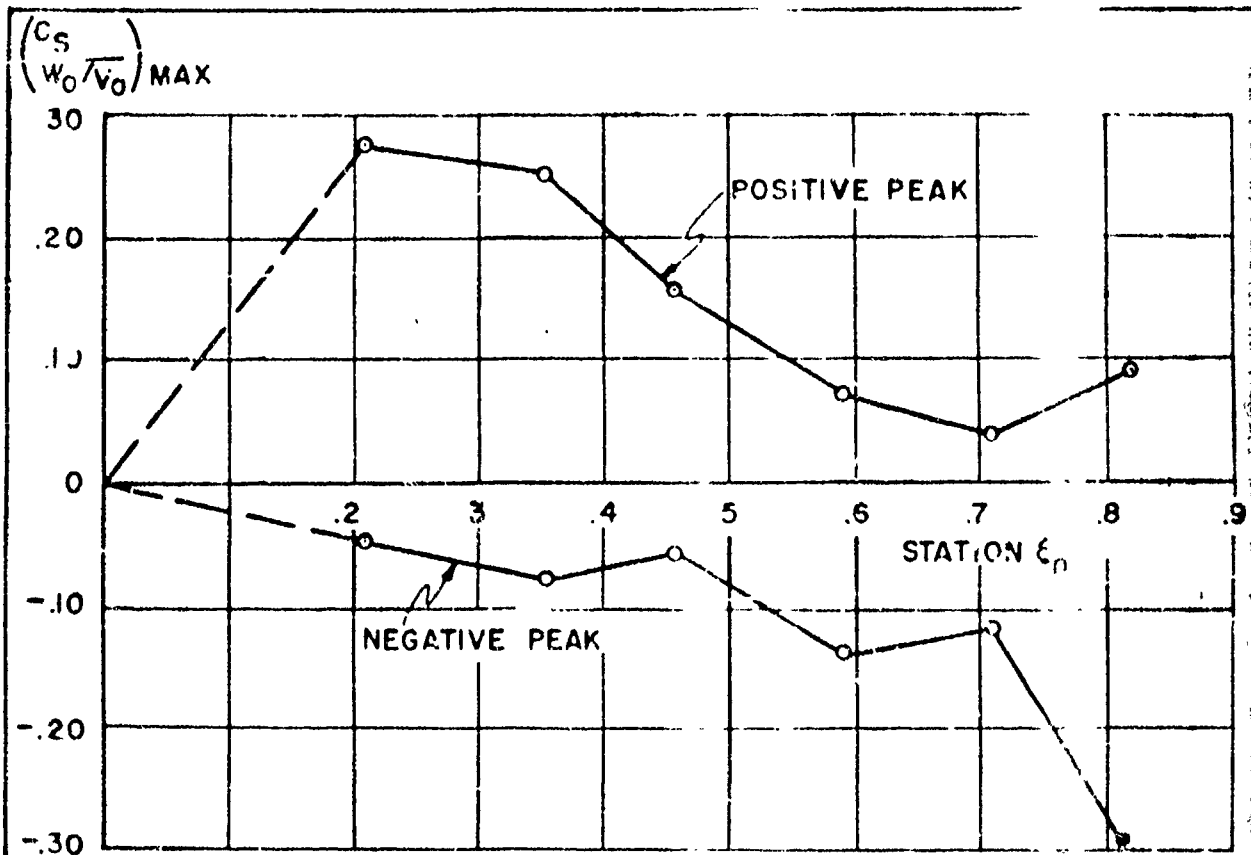

FIG. 26 PEAK VALUES OF THE SHEAR COEFFICIENT DUE TO 1-COS GUST, $S_G = \frac{1}{2}$

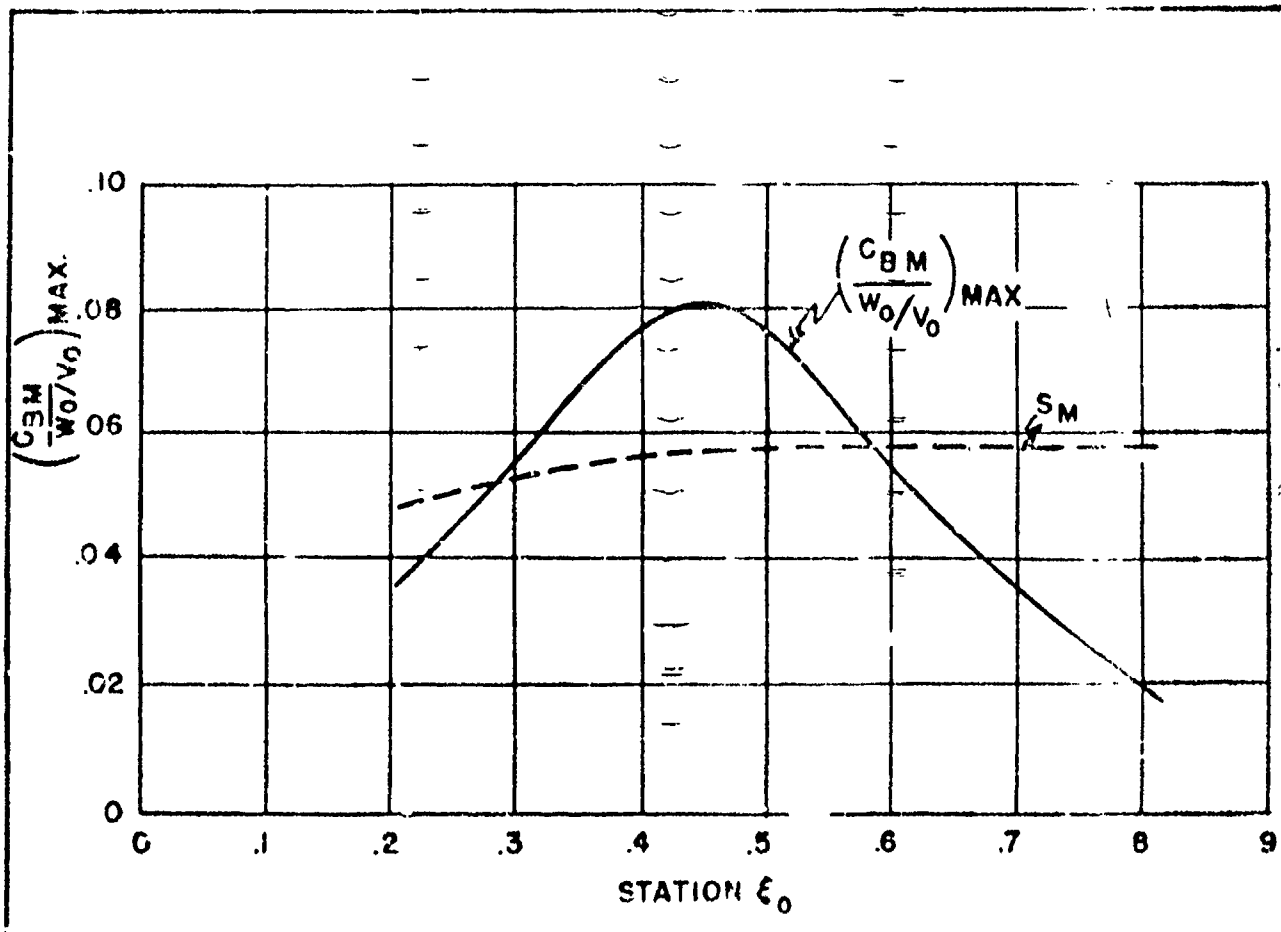

FIG. 27 ENVELOPE OF MAXIMUM BENDING MOMENT COEFFICIENT DUE TO 1-COS GUST, $S_G = \frac{1}{2}$

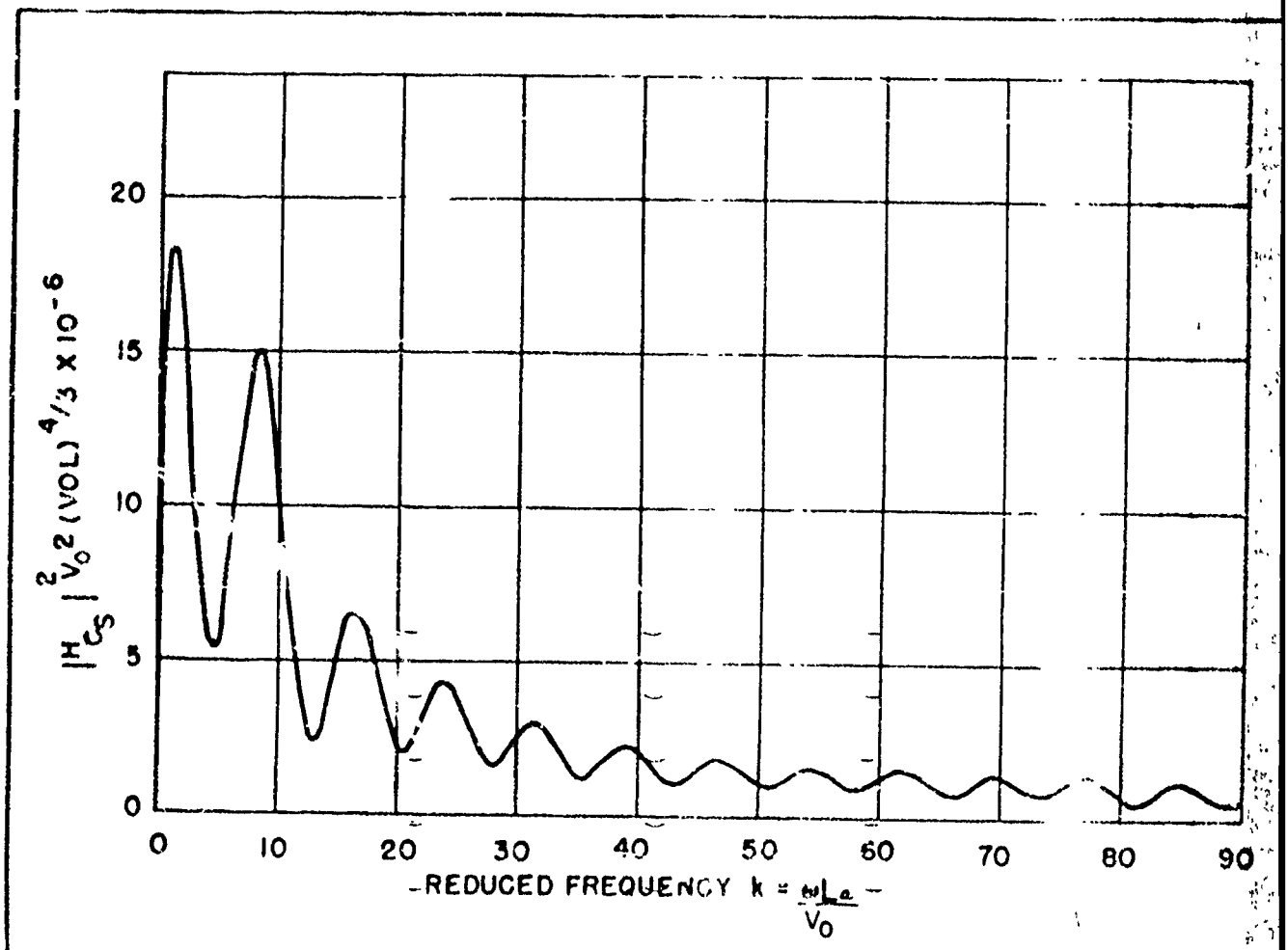

FIG. 28 TRANSFER FUNCTION WITH RESPECT TO SHEAR COEFFICIENT AT $\xi_0 = .8171$

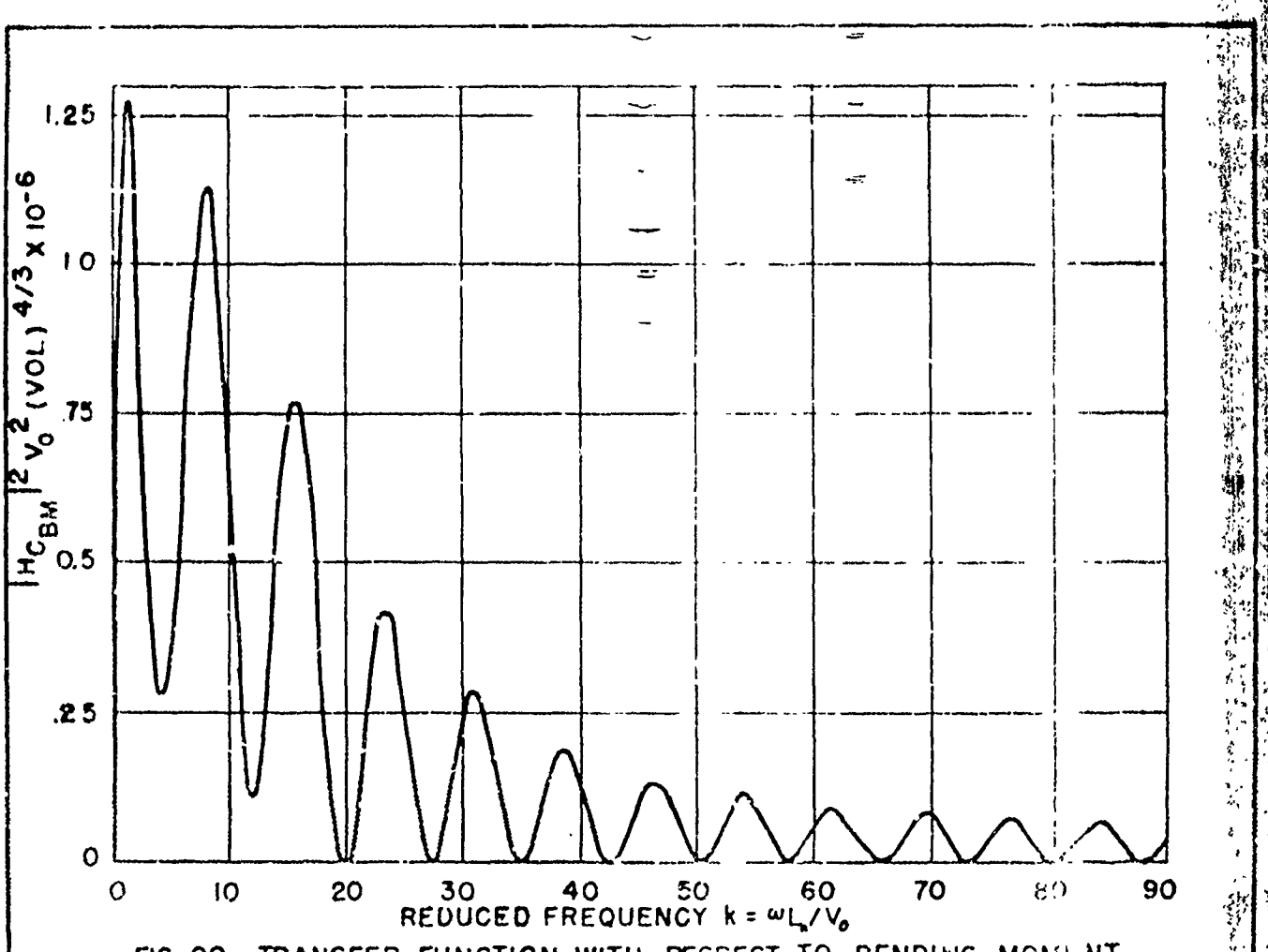

FIG. 29 TRANSFER FUNCTION WITH RESPECT TO BENDING MOMENT COEFFICIENT AT $\xi_0 = .4572$

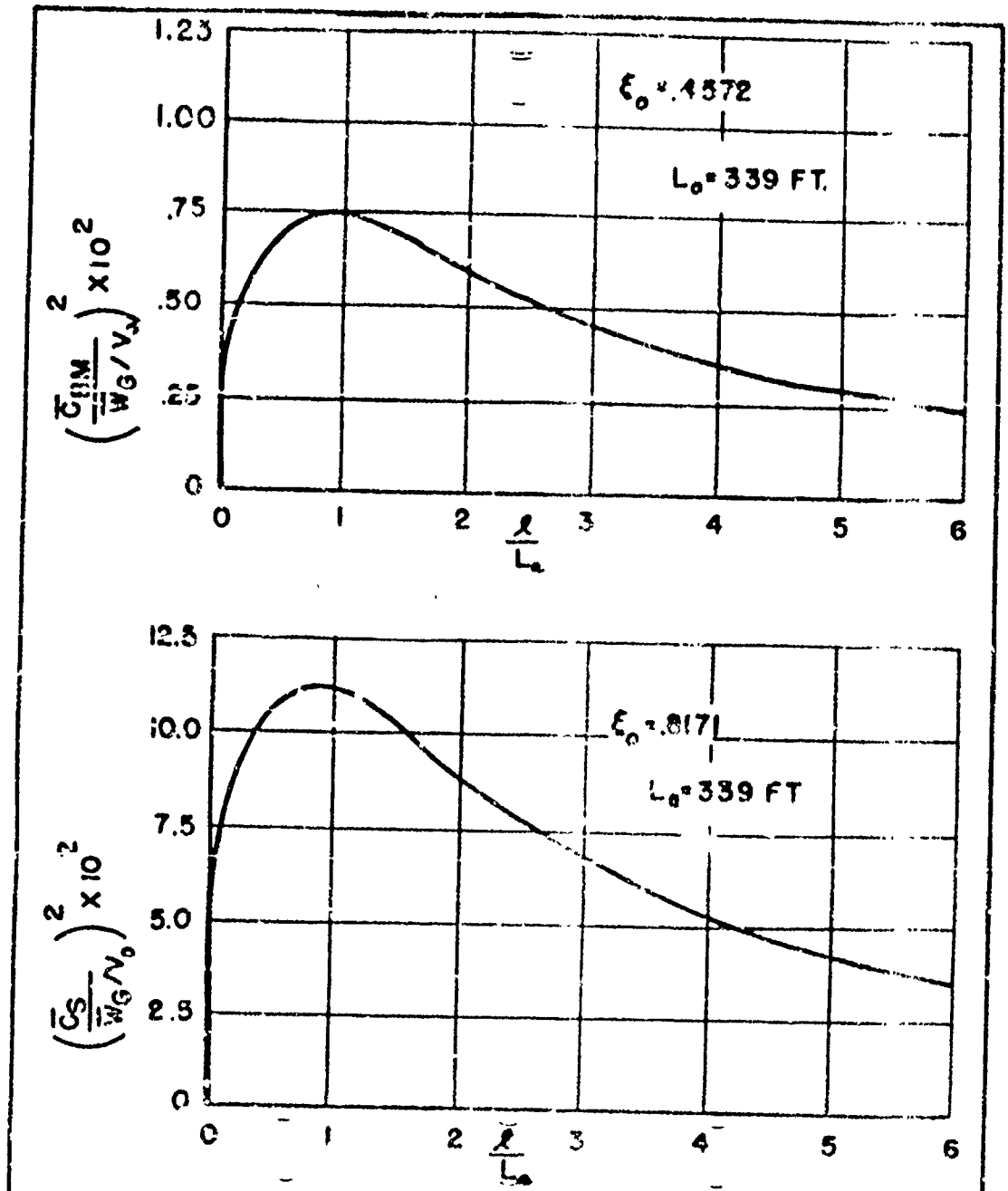

FIG. 30 MEAN SQUARE VALUES OF SHEAR AND BENDING MOMENT COEFFICIENTS